



A two-dimensional boundary element method for floating cylinders of arbitrary shape in frequency domain with power take off and second order predictions

Master thesis

M.J.E. Gabriel

Master Thesis

A two-dimensional boundary element method for floating cylinders of arbitrary shape in frequency domain with power take off and second order predictions

M.J.E. Gabriel

In partial fulfilment of the requirements for the degree of

Master of Science
in Marine Technology

at the Delft University of Technology,
to be defended publicly on Friday 29 November 2019.

Daily supervisor
Dr. ir. P.R. Wellens

Thesis committee:	Dr.ir. P.R. Wellens	Delft University of Technology
	Dr.ir. H.J. de Koning Gans	Delft University of Technology
	Dr. H.S. Seyffert-Cenzer	Delft University of Technology
	Dr.ir. M.J.B.M. Pourquoi	Delft University of Technology

Abstract

A two-dimensional (2D) panel method is developed to find the first and second order wave forces acting on a semi-submerged cylinder in regular waves. The panel method is based on potential flow and the waves are modeled for both finite and infinite water depth. The motion is limited to heave, but allows for extensions to other modes as well. It uses boundary conditions for floating body dynamics with Neumann and mixed type boundaries on the surfaces. The waves are generated and the reflection of the waves is suppressed by generating absorbing boundary conditions (GABC) on the radiation surfaces. The model is used to investigate the hydrodynamics of an oscillating buoy wave energy converter (point energy converter). For this, an analytical solution of the optimal damping is used. The method uses panels along all boundaries to solve the boundary conditions. The model can be used for any time-harmonic free surface flow problem.

A second order wave running through the domain is successfully modelled, without the interference of a body. Challenges of a second order model with body are explained. The boundary element method has innate challenges finding the correct solution to tangential flows on the panels and spatial derivatives of the velocity, which are required for the second order solutions.

Highlights

- Diffraction and radiation problems in boundary element methods for any 2D shape on the free surface are modeled.
- Two-dimensional generating absorbing boundary conditions are applied to free surface waves.
- The energy balance for a floating body with power take off with the combined radiation and diffraction problem is modeled.
- Power predictions for 2D floating devices with power take off in waves is found.
- Modelling a second order running wave through a fluid domain.
- Second order theory and challenges are explained for further model improvements.

Preface

This master thesis concludes the many years I have studied in Delft. It has not been the most common path. I started off with a Bachelor study at Industrial Design Engineering. I filled up my free time sailing and with social activities of the sailing association Broach. During my bachelor I found out that I was missing a technical challenge. I chose to apply for a bridging program to Maritime Engineering, as this was both a technical study and I could combine this with my passion for ships. During my master program I found more and more affinity towards the more technical courses, which led to my choice to switch from the ship design track to the hydrodynamics track, a good choice. This thesis is therefore a representative conclusion for my journey through my studies, as it is the result of the technical challenge I was looking for.

I would like to thank the people who helped me achieving this result. I would like to thank Peter Wellens, my supervisor at the TU Delft. Even though Peter appears to always be busy, he consistently found time to have in depth discussions and I always felt welcome to simply walk into his office with either questions or new exciting results. Peter also always knew how to trigger my motivation whenever I felt the challenges were becoming slightly overwhelming. I would also like to thank Henk de Koning Gans, who was a great help with his knowledge and experience with boundary element methods. From both these people I felt there was great enthusiasm about my work and this helped to push me whilst developing the model described in my thesis.

I would also like to thank my friends. They provided me with distractions throughout my studies, making my time in Delft a very joyful experience. I would like to thank Joren and Daan for our great years as a sailing team. Also I would like to thank Joost and Rogier for our many social interactions, sometimes only with digital communications. Michel, Wick, Jacob, Michiel and Derk, thank you for our many coffee breaks and study sessions. Without these breaks, often filled with many discussions, I would not have been the engineer I am today.

My family also deserves special thanks. Although neither my parents Chris and Monique or my sister Emmy live in the same country as me, I always enjoy sharing and following news through the family chat group. They are always ready to help me when I ask for support, albeit for my thesis or other matters. Finally I would like to thank my girlfriend Jitske. She fills my weekly life with the joy of our messages and our common weekends in Groningen or Delft. She sometimes reminds me of my responsibilities when I need to hear it and other times provides me with much needed distractions and love. I am grateful for the time we spend together and the way she always supports me.

Maarten Gabriel

Contents

1 Problem Definition	1
2 Literature review	2
2.1 Potential wave theory	2
2.2 Boundary element methods	4
2.3 Wave energy converters	5
3 Objectives	7
3.1 Research question	7
3.2 Approach	7
3.3 Overview	8
4 Background theory	9
4.1 Potential Wave Theory	9
4.2 Floating bodies	12
4.3 Forces and Pressures	13
4.4 Power prediction and optimal damping	15
4.5 Boundary Element Theory	16
5 Linear problem	18
5.1 Problem description	18
5.2 Boundary conditions	19
5.3 Generating absorbing boundary condition	19
5.4 Discretization	20
5.5 Coupling radiation and diffraction problem	22
5.6 Validation and verification	23
5.7 Results	27
5.8 Conclusions	34
6 Second order problem	35
6.1 Non-linear model	35
6.1.a Boundary conditions	35
6.1.b Discretization	36
6.2 Results	37
6.3 Conclusions	43
7 Conclusions and recommendations	44
7.1 Conclusions	44
7.2 Recommendations	45
Appendices	a
A Green Function	b
B Derivation Linear Potential	e
C Finite depth second order wave derivation	g
D Boundary element method	i

Definitions

Superscripts and subscripts

Φ is chosen as arbitrary symbol to serve as an example.

$\Phi_{[n]}$	Vector of length n
$\Phi_{[n,m]}$	Matrix of dimensions $n \times m$
$\Phi^{(1)}$	First order
$\Phi^{(2)}$	Second order
$\Phi(t)$	A function of t

Symbols

∇	differential operator	Φ	potential
Φ_I	incoming wave potential	Φ_D	diffracted wave potential
Φ_R	radiated wave potential	η	free surface elevation
ω	frequency	k	dimensionless frequency, wave number
t	time	\mathbf{u}	velocity vector
u	velocity in x-direction	v	velocity in y-direction
z	complex coordinate ($x + iy$)	A	incoming wave amplitude
p	pressure	ρ	density
g	gravitational acceleration	n_b	identity vector normal to body surface
β	coordinate of rotation	S	surface area
S_b	body surface	S_F	free surface area
S_R	radiation boundary surface	φ	space dependent potential
c	wave speed	B_0	bottom surface
M	mass	μ	added mass
λ	damping	K	spring stiffness
N	panel numbering	x_L	position of left radiation boundary
x_R	position of right radiation boundary	$a(t)$	complex motion of body
$\dot{a}(t)$	complex velocity of body	$\alpha(t)$	body motion
$\dot{\alpha}(t)$	body velocity	$\ddot{\alpha}(t)$	body acceleration
l	panel length	s	local panel coordinate
z_1	local panel position	z_a	local panel start coordinate
z_b	local panel end coordinate	z_c	local panel center
P	potential influence matrix	Q	normal velocity influence matrix
G	influence matrix of d/dy of the potential	S_a	waterplane area
C	complete boundary condition matrix	K	known wave parameter matrix
q	source strength	F	force
ϵ	phase	ζ	response amplitude operator (RAO)
P_I	incoming wave power	P_A	absorbed power
P_R	radiated wave power	P_T	transient wave power
η_h	hydrodynamic efficiency	R	radiation coefficient
T	transmission coefficient	$\frac{D}{Dt}$	material derivative operator
V	velocity influence matrix	G	green function

Chapter 1

Problem Definition

Wave energy converters (WECs) use the energy available in waves to generate power. A prediction needs to be made how much power can be absorbed from the incoming waves. A model is made to estimate this power absorption, since full scale testing is not feasible in a design stage. The model has to predict the reality as closely as possible, but there will always be assumptions to model all complicated real world phenomena. There is existing theory on finding the average power using linear potential theory. This thesis will elaborate on that theory and find the contributions of the second order phenomena. This should improve the model to better match reality, as steeper waves can be modelled more accurately and the second order interaction between different waves an frequencies is included.

Chapter 2

Literature review

In this chapter the literature related to the present research will be presented and discussed. This will be done in multiple parts, discussing key features of the research.

Firstly, a literature review on potential theory of gravity waves is outlined, including second order effects. A literature study on floating bodies is presented including results from theory and experiments. Secondly, existing literature on boundary element methods (BEM's) will be discussed. The literature research will conclude with wave energy converters.

2.1 Potential wave theory

Since the problem is solved with a boundary element method, only potential flow theories are of interest in this research. Potential theory is based on two fundamental equations: the conservation of mass and the conservation of momentum. **The objective is not to research new non-linear wave theories.** Existing non-linear wave theory is used to perform the research.

Linear wave theory

For linear potential theory all equations are linearized, meaning higher than first order terms are neglected. This results in harmonic waves propagating along the surface. The pressures in the flow can be calculated with the Bernoulli equation. It is assumed the waves are not steep, and are large enough to neglect surface tension. This theory is also known as the Airy wave theory. The potential function of the Airy wave is seen below. In order to satisfy the boundary conditions, the dispersion relation must also hold, as shown in Eq. (2.2). This dispersion relation couples the frequency and wavelength of the waves. This also means long waves travel faster than short waves and deep water waves travel faster than shallow water waves, which is also seen in reality [10]. The wave speed is defined as $c = \omega/k$.

$$\Phi^{(1)} = \frac{A g \cosh(k(h+y))}{\omega \cosh(k h)} \cos(\omega t - kx) \quad (2.1)$$

$$\omega^2 = k g \tanh(k h) \quad (2.2)$$

Non-linearity

In order to solve a non-linear problem, it is common to use perturbation theory. This describes a function or solution on different order terms. This was first done by Stokes in 1847 [24] for free surface gravity waves. This was repeated by [22] for waves with infinite water depth.

$$A = A^{(0)} + \varepsilon A^{(1)} + \varepsilon^2 A^{(2)} + \dots \quad (2.3)$$

In this equation, A is the perturbation series approximating the real function. ε is typically a small term (for waves it is the wave steepness), so that higher order terms become smaller as the order increases.

Therefore, an approximate solution is found by truncating the series, which could for example result in only first order terms ($A = A^{(0)} + \varepsilon A^{(1)}$), as done by the linear potential wave theory, or second order terms ($A = A^{(0)} + \varepsilon A^{(1)} + \varepsilon^2 A^{(2)}$), as done for the second order wave theory.

An index to find the non-linearity for waves in finite water depth is the Ursell number. It is defined as the steepness/(relative depth)³. The higher the Ursell number, the more non-linear a wave is going to behave.

$$N_{Ursell} = \frac{A/L}{(h/L)^3} = \frac{AL^2}{h^3} \quad (2.4)$$

The results for the second order potential found in this thesis is derived in Appendix C, as shown by Stokes [24].

$$\Phi^{(2)} = \frac{3A^2\omega}{8} \frac{\cosh(2k(h+y))}{\sinh^4(kh)} \sin(2(\omega t - kx)) \quad (2.5)$$

Bi-chromatic waves

Longuet-Higgins [18] showed that for second order bi-chromatic second order waves a sum and difference frequency appear to satisfy the dynamic boundary condition at the free surface. This results in a 2D velocity potential as shown in Eq. (2.6) by Dalzell [6], with a as amplitude and A as coefficients shown in Eq. (2.7b) and Eq. (2.7c). As the problem is 2D, the relative angle between the waves ($\theta_1 - \theta_2$) is assumed 0, as the propagating direction of the wave can only be in x direction. Interestingly, this results in there being no sum terms in the potential.

$$\Phi = \sum_{i=1}^n \left(\sum_{j=1}^n a_i a_j A_p^\infty e^{(k_i+k_j)z} \sin(\Psi_i + \Psi_j) + a_i a_j A_m^\infty e^{(k_i-k_j)z} \sin(\Psi_i - \Psi_j) \right) + \frac{g a_i}{\omega_i} e^{k_i z} \sin(\Psi_i) \quad (2.6)$$

$$\Psi_i = k_i x - \omega_i t \quad (2.7a)$$

$$A_p^\infty = \frac{\omega_i \omega_j (\omega_i + \omega_j) (1 - \cos(\theta_1 - \theta_2))}{(\omega_i + \omega_j)^2 - g|k_i + k_j|} \quad (2.7b)$$

$$A_m^\infty = \frac{\omega_i \omega_j (\omega_i - \omega_j) (1 + \cos(\theta_1 - \theta_2))}{(\omega_i - \omega_j)^2 - g|k_i - k_j|} \quad (2.7c)$$

Floating bodies

If a body is floating within the waves, some boundary conditions are added to the system of equations. The water particles can not enter the body, so there is a no-penetration boundary condition on the body. Also, the body has its own equations of motion which have to be introduced to the system. The fluid domain with the additional boundary condition can be solved in different ways. There is an option to solve for a body fully analytically. This has been done for a cylinder by Dean [7] and Ursell [27], [28] up to first order. The mathematics required to solve this are extensive. Ogilvie [23] extended this theory to include second order forces on a stationary and free to respond submerged cylinder. The application for these theories is limited, as not many geometries allow for a fully analytical solution. Discretization offers additional opportunities in solving these problems, as will be discussed later.

2.2 Boundary element methods

A method to find waves and pressures in a fluid domain is to discretize the problem with a lot of small panels. Boundary element methods or also named panel methods exist that use this technique. Sources are used to satisfy the boundary condition on each panel. This results in matrix calculations solving the boundary conditions on each panel and thereby also giving the entire velocity field around the object. Currently, many examples of functioning panel methods exist, with Delfrac, Rapid, and WAMIT being only a small example of them.

Frank [9] used sources of large complexity which use Green functions to solve the boundary conditions at the free surface and at infinity. A more detailed explanation of Green functions is shown in the appendix. The advantage of using these complicated Green functions is that only the body surface itself needs to contain panels. The research done by Frank is useful for cylinders in or below the free surface. The limitations are that it is done in two dimensions and only solves the linear potential flow problem. More on linear Green functions is found in Appendix A.

A more sophisticated example is the work done by Kim and Yue [15], [14]. They use a complicated Green function to solve the second order diffraction problem and find the body motions and pressures. This is also done in three dimensions. The software WAMIT uses the methods from this work to calculate the second order flow around floating bodies.

A different approach is taken by Yeung [31]. Instead of using a complicated Green function to solve for the boundary conditions, simpler sources are used on the panels. The boundary conditions at the free surface and at infinity are solved by having panels on the free surface and including a radiation boundary. This increases the amount of panels needed, but reduces the complexity of the calculations. The work done by Yeung is in two and three dimensions for waves radiating away from a moving body.

A boundary element method can be in a time-domain or a frequency domain. A time domain calculates all pressures for a time step, and differentiation in time is done with different time steps. This allows to calculate the development of a problem in time. However, when a problem is fully harmonic in time, a frequency domain can be used. This requires only one single calculation to solve the entire behaviour, where every value is oscillating and represented with an amplitude and phase. This is a lot faster than time domain calculations, since only one matrix equation has to be solved. An example of time domain is the work done by Ballast [3], who uses numerical beaches in a time domain to calculate higher order pressures. A frequency domain is used by Yeung [31], who solves a linear, 2D radiation problem.

Objectives

This report will focus on a two-dimensional method that solves both the diffraction and radiation problems. It will combine the method of Yeung with panels on all boundaries with the possibility to add incoming waves. It will also combine both methods for a power prediction of a power take off in the system. An additional objective is to add non-linear effects up to second order for both the diffraction and radiation problem, to increase the accuracy of the BEM and power prediction.

2.3 Wave energy converters

Introduction

There are many forms of WECs. The goal is always to transform mechanical energy from the waves to a form of electrical energy that can be transported and used. An overview is given by the European Marine Energy Centre [2]. The different kinds of WECs are seen below:

- Attenuator
- Oscillating wave surge converter
- Oscillating water column
- Overtopping/terminator device
- Submerged pressure differential
- Bulge wave
- Rotating mass
- Point absorber

The attenuator uses the difference in free surface level and buoyancy to have different sections hinge with respect to each other. This relative rotation can generate power. The oscillating wave surge converter is a plate which moves back and forth with the wave surge, pivoting around a joint on the sea bed. The oscillating water column is a partially submerged hollow structure which uses the rising and falling water level due to the waves to compress and decompress the air within. This can then drive a turbine. The overtopping device captures the elevated water from waves and uses the difference in hydro-static pressure when this is returned to the sea. The submerged pressure differential heaves with the pressures just below the free surface. A bulge wave is a rubber tube filled with water, in which bulges appear and travel through the tube increasing in size. At the end of the tube they drive a turbine. The rotating mass is a device that uses the motion in pitch to rotate a mass inside, which generates power.

Finally, the point absorber is a floating structure which moves with the waves, generating power. An example is shown in Fig. 2.1. Many configurations of the device are possible, and multiple degrees of freedom can be exploited. Somewhere in the system a power take off (PTO) can be installed to transform the mechanical energy to electrical energy. Point absorbers have some advantages over other types of WECs. They can absorb wave energy from all directions and they have a relatively simple design. This also makes them more cost effective [13].

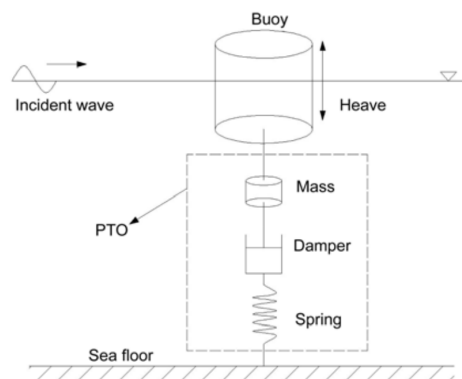


Figure 2.1: Schematic display of a heaving point absorber WEC with PTO system [5]

Mass-spring-damper system

A linear mass-spring-damper system is used to define the motion of a point absorber. The terms from the mass-spring-damper can be added to a classical equation of motion. Rewriting this with added mass, radiated wave damping, wave pressure and mass-spring-damper terms, gives:

$$[M + \mu] \ddot{\mathbf{X}} + [\lambda + \lambda_{PTO}] \dot{\mathbf{X}} + [C + K] \mathbf{X} = \mathbf{F} \quad (2.8)$$

where M , B and C are mass and hydro-static terms as derived earlier, A is the added mass matrix and B the radiated and diffracted waves damping matrix. λ_{PTO} is the PTO damping coefficient and K the mechanical spring stiffness. These two final values can be tuned to generate a desired response of the system. The non-linear contributions found by the BEM can be included in this equation, as they are separated with perturbation theory. For a certain optimal damping coefficient, the most power is absorbed by the PTO. The obtained power is seen in equation Eq. (2.9) by Teillant [25].

$$P_d = \lambda_{PTO}(t) \dot{x}(t)^2 \quad (2.9)$$

Most existing theories are based on a linear system, and must be expanded for non-linearity. For example, a hydraulic PTO is highly non-linear as shown by Falcao, [8]. This can be controlled to behave linearly, but a non-linear damping possibility in the model allows for a better evaluation.

Chapter 3

Objectives

3.1 Research question

The goal of the research is to develop a first order method for the estimation of the power taken off by a WEC which is suitable to be extended to second order. This will build on existing panel method technology. The research question is stated as

How can the second order effects on the power prediction of WEC be determined?

Secondary goals are established to answer the main research question. Answering these will lead to the answer of the overall research question, in a step-wise approach.

1. How can the fluid domain with body be described?
2. How can a wave be added to the fluid domain?
3. How can the produced power of the moving body be determined??
4. How can second order effects be implemented in the model?

3.2 Approach

The result of this research will be a 2D model evaluating the behaviour of a point absorber WEC up to first order with predictions and recommendations for a second order model. This will be evaluated for water of arbitrary depth, and it will be done within a frequency domain. Some differences between a first and second order model will be presented, and the relevance of the additional complications in the analysis will be discussed.

The process will be divided by the different sub goals stated in 3.1. These will be discussed subsequently.

First order model

First, a 2D boundary element method will be made. This is done to create the comparison to first order, and to give the overview of a linear method, which will be simpler to understand than a higher order method. Existing methods can be used, and no additional Green functions need to be derived.

A method needs to be found to add incoming waves into a 2D frequency domain. This will be done by finding comparable methods from other numerical models. When completed, the model must be able to solve both the diffraction and radiation problem to find the complete power prediction.

finally, the power must be predicted for the wave energy converter, finding the ideal damping for the power take-off. Up to this point, only linear components are regarded.

Second order predictions

A start is made at predicting the second order contributions in the model. This is done by finding the relevant second order theory and implementing this in the existing linear model. A look will be had at the added difficulties and challenges, but also at the possibilities of the model to be expanded to second order.

3.3 Overview

The objective is to develop a method in 2D that can quickly and more realistically predict the efficiency of a WEC. This will improve the design possibilities for a wave energy converter.

Overview Objectives		
	State of the art	Beyond state of the art
Non-linear wave theory	Defined up to very high orders [22], [24]	Use second order potential theory to find the second order contributions to the produced power
Boundary element methods	Second order with Green function in 3D [14], Radiation problem in 2D with panels on all boundaries in frequency domain [31]. Radiation and diffraction problem in time domain 3D [3] with numerical beaches	Solve both diffraction and radiation problem in 2D in the frequency domain. Combine these solutions to find the optimal power take off. Include second order effects
Wave energy converters	Use a variety of methods to find the hydrodynamic properties. Then evaluate the ideal power take off [13], [29].	Decrease time needed to find an accurate solution for the optimal damping and efficiency.

The table below shows the comparison to other existing literature with boundary element methods:

Table 3.1: State of the art BEM

	2D	3D	Incoming waves	Simple sources	Frequency domain	Couple incoming waves with radiated waves	Second order
Kim, Yue (1990) [14]	No	Yes	Yes	No	No	No	Yes
Yeung (1973) [31]	Yes	Yes	No	Yes	Yes	no	No
Frank (1967) [9]	Yes	No	Yes	No	Yes	No	No
Ballast (2004) [3]	No	Yes	Yes	Yes	No	Yes	Yes
This research	Yes	No	Yes	Yes	Yes	Yes	Yes

Chapter 4

Background theory

This chapter will explain some of the fundamental theories on which the developed model is built. The definitions in this chapter will be referred to throughout the rest of the report, and form the basis of the research.

4.1 Potential Wave Theory

Linear Wave Theory

Different annotations of the wave potential are often used throughout different literature, which asks for some clarification on the definitions used in this report. Also, the complex potential will be defined in this chapter.

Harmonic propagating wave

A wave propagating in the positive x-direction is referred to as a right going wave [10]. It must hold the conditions for an ideal fluid, mass conservation (Eq. (4.1a)) and the kinematic and dynamic boundary condition as given below (Eq. (4.1b)). The no-penetration boundary condition of the bottom surface is described in Eq. (4.1c).

$$\nabla^2 \Phi = 0 \quad (4.1a)$$

$$\frac{\partial \Phi}{\partial y} = \frac{\partial \eta}{\partial t} \quad y = 0 \quad (4.1b)$$

$$\frac{\partial \Phi}{\partial y} = 0 \quad y = -h \quad (4.1c)$$

The resulting wave potential is seen here, found with the condition that the free surface behaves like a sine wave. The derivation of this potential can be found in the appendix.

$$\eta = A \sin(\omega t - kx) \quad (4.2a)$$

$$\Phi = \frac{A g}{\omega} \frac{\cosh(k(h+y))}{\cosh(kh)} \cos(\omega t - kx) \quad (4.2b)$$

The velocities in x and y direction can be derived from this potential:

$$\frac{\partial \Phi}{\partial x} = u = A \omega \frac{\cosh(k(h+y))}{\cosh(kh)} \sin(\omega t - kx) \quad (4.3a)$$

$$\frac{\partial \Phi}{\partial y} = v = A \omega \frac{\sinh(k(h+y))}{\cosh(kh)} \cos(\omega t - kx) \quad (4.3b)$$

Left going wave

A wave propagating in the negative x-direction is called a left going wave. This is defined slightly differently as the right going wave:

$$\Phi = \frac{A g}{\omega} \frac{\cosh(k(h+y))}{\cosh(kh)} \cos(\omega t + kx) \quad (4.4)$$

Infinite Depth

For infinite depth, a part of the potential can be simplified, leading to the potential as shown below.

$$\frac{\cosh(k(h+y))}{\cosh(kh)} = \frac{e^{kh+ky} + e^{-kh-ky}}{e^{kh} + e^{-kh}} \quad (4.5a)$$

$$h \rightarrow \infty : e^{kh} = \infty, e^{-kh} = 0 \quad (4.5b)$$

$$\frac{e^{kh+ky}}{e^{kh}} = e^{ky} \quad (4.5c)$$

$$\Phi = \frac{A g}{\omega} e^{ky} \cos(\omega t + kx) \quad (4.6)$$

Complex potential

The sine and cosine components can be written in complex form, as shown below.

$$\Phi = \frac{A \omega}{k} \frac{\cosh(k(h+y))}{\cosh(kh)} e^{-ikx} e^{i\omega t} \quad (4.7)$$

$$u = -i A \omega \frac{\cosh(k(h+y))}{\cosh(kh)} e^{-ikx} e^{i\omega t} \quad (4.8a)$$

$$v = A \omega \frac{\sinh(k(h+y))}{\cosh(kh)} e^{-ikx} e^{i\omega t} \quad (4.8b)$$

Second order wave theory

$$\nabla^2 \Phi = 0 \quad (4.9a)$$

$$\frac{p}{\rho} = \frac{\partial \Phi}{\partial t} + |\nabla \Phi|^2 + g\eta = 0 \quad (4.9b)$$

$$\frac{\partial \eta}{\partial t} = \frac{\partial \Phi}{\partial y} + \frac{\partial \Phi}{\partial x} \frac{\partial \eta}{\partial x} \quad (4.9c)$$

The potential must again satisfy the Laplace equation (Eq. (4.9a)), and the dynamic boundary condition (Eq. (4.9b)). This prescribes a constant atmospheric pressure along the free surface. It is evaluated from the unsteady Bernoulli equation along the free surface streamline [22]. This can be done since a characteristic of potential flow is that along a streamline the pressure does not change [17]. The kinematic boundary condition, which describes that a fluid particle will remain on the free surface, is seen in Eq. (4.9c).

The resulting second order wave potential is seen in Eq. (4.10). Interestingly, for a single wave this is the same result as for the first-order wave.

$$\Phi = \frac{g A}{\omega} e^{ky} \sin(-kx + \omega t) + O(A^3) \quad (4.10)$$

The free surface elevation is given in Eq. (4.11). The second term in the equation is not an added free surface wave, but locked to the first order wave. This is also called a Stokes wave. It can be seen in Fig. 4.1. The Stokes wave has higher and shorter peaks, but also less deep and wider troughs.

$$\eta = A \cos(kx - \omega t) + \frac{1}{2} k A^2 \cos(-2kx + 2\omega t) + O(A^4) \quad (4.11)$$

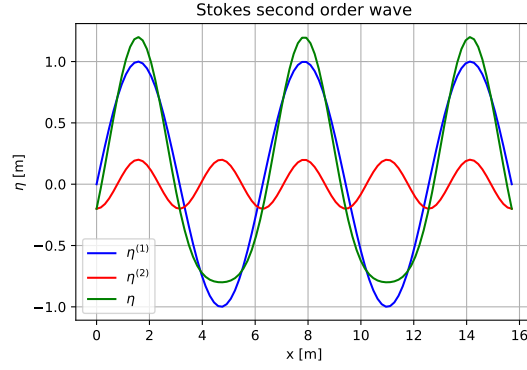


Figure 4.1: Second order wave

Derivation second order potential

The derivation for the non-linear wave potential will be given here. This is done by finding a solution for the boundary conditions, as shown by Newman [22]

Replacing the kinematic boundary condition with the material derivative of the pressure gives the following exact boundary condition at the free surface. The derivation of the boundary condition is found in the appendix. The final term is neglected as this is third order. An expression for η is seen in Eq. (4.14), evaluated from the dynamic boundary condition.

$$\frac{Dp}{Dt}(y = \eta) = 0 \quad (4.12)$$

$$\frac{\partial^2 \Phi}{\partial t^2} + g \frac{\partial \Phi}{\partial y} + 2 \nabla \Phi \cdot \nabla \frac{\partial \Phi}{\partial t} + \frac{1}{2} \nabla \Phi \cdot \nabla (\nabla \Phi \cdot \nabla \Phi) = 0 \quad (4.13)$$

$$\eta = -\frac{1}{g} \left(\frac{\partial \Phi}{\partial t} + \frac{1}{2} \nabla \Phi \cdot \nabla \Phi \right) \quad (4.14)$$

To approximate the second order potential with the free surface boundary as expressed in Eq. (4.13), a Taylor expansion is made around $y = 0$. The first and second order components can be split. A more detailed explanation of this derivation is found in Appendix B.

$$\Phi(x, \eta, t) = \Phi(x, 0, t) + \eta \frac{\partial \Phi}{\partial y} \Big|_{y=0} \quad (4.15a)$$

$$\Phi = \Phi^{(1)} + \Phi^{(2)} \quad (4.15b)$$

$$\frac{\partial^2 \Phi^{(1)}}{\partial t^2} + g \frac{\partial \Phi^{(1)}}{\partial y} = 0 \quad (4.15c)$$

$$\frac{\partial^2 \Phi^{(2)}}{\partial t^2} + g \frac{\partial \Phi^{(2)}}{\partial y} = -2 \nabla \Phi^{(1)} \cdot \nabla \frac{\partial \Phi^{(1)}}{\partial t} + \frac{1}{g} \frac{\partial \Phi^{(1)}}{\partial t} \frac{\partial}{\partial y} \left(\frac{\partial^2 \Phi^{(1)}}{\partial t^2} + g \frac{\partial \Phi^{(1)}}{\partial y} \right) \quad (4.15d)$$

$$\Phi^{(2)} = \frac{3 A^2 \omega \cosh(2k(h+y))}{8 \sinh^4(kh)} e^{-2ikx} e^{2i\omega t} \quad (4.16)$$

The result of the second order potential is seen above. $\Phi^{(2)}$ is 0 for deep water, since it analytically reduces to 0. This means the first order potential as seen in Eq. (4.6) is a solution to the second order boundary problem in infinite depth.

$$\eta = -\frac{1}{g} \left(\frac{\partial \Phi}{\partial t} + \frac{1}{2} \nabla \Phi \cdot \nabla \Phi \right) \Big|_{y=0} + \eta \frac{\partial}{\partial y} \left(-\frac{1}{g} \left(\frac{\partial \Phi}{\partial t} + \frac{1}{2} \nabla \Phi \cdot \nabla \Phi \right) \right) \Big|_{y=0} \quad (4.17a)$$

$$\eta = A \cos(kx - \omega t) + \frac{1}{2} k A^2 \cos(2kx - 2\omega t) + O(A^4) \quad (4.17b)$$

The free surface elevation for infinite depth can be found by another Taylor expansion around $y = 0$ and is given in Eq. (4.17b). Here, Φ as in Eq. (4.2b) is substituted. The second term in the equation is not an added free surface wave, but locked to the first order wave. The solution for finite depth is seen in Eq. (4.18), as derived by Stokes [24].

$$\eta = A \cos(kx - \omega t) - kA^2 \frac{(e^{kh} + e^{-kh})(e^{2kh} + e^{-2kh} + 4)}{2(e^{kh} - e^{-kh})^3} \cos(2kx - 2\omega t) \quad (4.18)$$

4.2 Floating bodies

With floating bodies in waves, a distinction is made between diffracted waves and radiated waves. The diffracted wave is a reflection from the incoming wave on the body surface, to satisfy the no-penetration condition. The radiated waves originate from the motion of the body, also satisfying the no-penetration condition on the body surface.

Diffracted wave

To solve the diffracted wave, the no-penetration boundary condition has to be satisfied at the body surface. This holds for each order n in the perturbation series. The previously defined wave potential Φ will now be named Φ_I , for the incoming wave.

$$\frac{\partial \Phi_I^{(n)}}{\partial n_b} = -\frac{\partial \Phi_D^{(n)}}{\partial n_b} \quad (4.19)$$

The diffracted wave is split in different order terms, as seen in Eq. (4.20a). The challenge arises when solving the second order term for the free surface boundary condition. Eq. (4.20b) and Eq. (4.20c) also hold for Φ_D , since it is still a water wave. To solve this problem, Molin [21] showed that both a locked and free wave must be included in the diffraction potential for a second order problem.

$$\Phi_D = \Phi_D^{(1)} + \Phi_D^{(2)} \quad (4.20a)$$

$$\nabla^2 \Phi_D = 0 \quad (4.20b)$$

$$g \frac{\partial \Phi_D^{(2)}}{\partial y} + \frac{\partial^2 \Phi_D^{(2)}}{\partial t^2} = A^{(2)} \quad (4.20c)$$

$$A^{(2)} = -\frac{\partial^2 \Phi_I^{(2)}}{\partial t^2} - g \frac{\partial \Phi_I^{(2)}}{\partial y} + 2\nabla \Phi^{(1)} \cdot \nabla \frac{\partial \Phi^{(1)}}{\partial t} + \frac{1}{g} \frac{\partial \Phi^{(1)}}{\partial t} \frac{\partial}{\partial y} \left(\frac{\partial^2 \Phi^{(1)}}{\partial t^2} + g \frac{\partial \Phi^{(1)}}{\partial y} \right) \quad (4.20d)$$

The detailed description of $A^{(2)}$ is found in Molin [21]. This is derived from the boundary condition at the free surface, as seen in Eq. (4.15d). A solution to this problem in 3D can be found in the work of Kim [14]. The diffracted and incoming wave will result in a bi-chromatic wave where the resulting wave is a semi propagating wave. This means both waves are travelling in the exact opposite direction. When deriving the wave potential given in Eq. (2.6), the resulting wave has a second order sum frequency term that is not dependent on position, but only on time. The potential can be seen in Eq. (4.21). Both waves share the same frequency and wave number, as the diffracted wave is a reflection of the incoming wave. Interestingly, this term also does not reduce with increasing depth. It is only a pressure term, since the spatial derivatives are always 0.

$$\Phi = \varphi^{(1)} e^{i\omega t} + \varphi^{(2)} e^{2i\omega t} \quad (4.21a)$$

$$\varphi^{(1)} = \frac{A_1 \omega}{g} e^{ky} e^{-ikx} + \frac{A_2 \omega}{g} e^{ky} e^{ikx} \quad (4.21b)$$

$$\varphi^{(2)} = A_1 A_2 \omega \quad (4.21c)$$

For finite depth, the same phenomenon occurs (Dalzell, [6]).

$$\Phi = \varphi^{(1)} e^{i\omega t} + \varphi^{(2)} e^{2i\omega t} \quad (4.22a)$$

$$\varphi^{(1)} = \frac{A_1 g \cosh(k(h+y))}{\omega \cosh(kh)} e^{-ikx} + \frac{A_2 g \cosh(k(h+y))}{\omega \cosh(kh)} e^{ikx} \quad (4.22b)$$

$$\varphi^{(2)} = 2A_1 A_2 \frac{\omega}{16} (3 + \coth^2(kh)) \quad (4.22c)$$

Radiated Waves

Radiated waves originate from the motion of the body. The boundary condition for radiated waves at the body is seen in Eq. (4.23).

$$\frac{\partial \Phi_R^{(n)}}{\partial n_b} = \hat{n}_b \cdot \mathbf{u}_b \quad (4.23)$$

The radiated waves depend fully on the motion of the body. Just like the incoming and diffracted waves, they have to fulfil the dynamic boundary conditions at the free surface and the Laplace equation. The motions of the body in 2D are limited to only three degrees of freedom: surge, heave and pitch. The equations of motion are derived from a linear momentum balance and an angular momentum balance. The resulting equation is as follows (Mei [19]), where the external damping term [B] is not part of the original equation from the author.

$$[M] \frac{\partial^2}{\partial t^2} \begin{bmatrix} X \\ Y \\ \beta \end{bmatrix} + [B] \frac{\partial}{\partial t} \begin{bmatrix} X \\ Y \\ \beta \end{bmatrix} + [C] \begin{bmatrix} X \\ Y \\ \beta \end{bmatrix} = -\rho \int_{S_B} dS \Phi_t \begin{bmatrix} n_1 \\ n_3 \\ n_5 \end{bmatrix} + \bar{F} \quad (4.24)$$

In this equation [M] contains terms of the mass and mass moment of inertia, with the center of gravity not coinciding with the center of rotation. [C] contains external forces and hydro-static forces and moments due to non-symmetry of the object. β is the angle around the z -axis. The term including Φ_t includes the added mass and damping of the floating object. A more detailed derivation can be found in Appendix A.

4.3 Forces and Pressures

To find the forces and pressures in the domain and on the body, use is made of the Bernoulli equation. It can be seen the pressure has different order terms, as shown up to second order in Eq. (4.26). $\eta^{(0)}$ is the water level at rest, which is chosen as 0 by definition.

$$\frac{p}{\rho} = \frac{\partial \Phi}{\partial t} + \frac{1}{2} |\nabla \Phi|^2 + \rho y \quad (4.25)$$

$$p^{(0)} = \rho g \eta^{(0)} = 0 \quad (4.26a)$$

$$p^{(1)} = \rho \frac{\partial \Phi^{(1)}}{\partial t} + \rho g \eta^{(1)} \quad (4.26b)$$

$$p^{(2)} = \frac{1}{2} |\nabla \Phi^{(1)}|^2 + \rho \frac{\partial \Phi^{(2)}}{\partial t} + \rho g \eta^{(2)} \quad (4.26c)$$

The forces on the body are the integration of the pressures along the body surface. For the body surface, a difference can be made for the static body surface of 0-th order, and higher order components which depend on the wetted surface on the body. This again depends on the wave height and body motion. We can make the distinction between surfaces as seen in Table 4.1 and Fig. 4.2. The same principle applies for higher order components of the body surface.

Table 4.1: Body surface distinction

Symbol	Description	Order
$S_b^{(0)}$	Body surface at equilibrium	0
$S_b^{(1)}$	Body surface with linear wave height and linear motion regarded	1
$S_a^{(0)}$	Waterplane area of body at equilibrium	0
$S_a^{(1)}$	Waterplane area of body with first order motions and wave heights	1

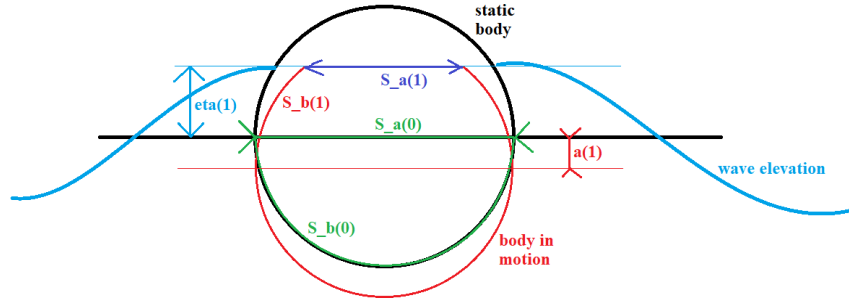


Figure 4.2: Surface distinction

With different orders in pressures and different orders in body surfaces, the following integrals provide the second order forces.

$$F^{(1)} = \int_{S_b^{(0)}} p^{(1)} + \int_{S_b^{(1)}} p^{(0)} \quad (4.27a)$$

$$F^{(2)} = \int_{S_b^{(0)}} p^{(2)} + \int_{S_b^{(1)}} p^{(1)} + \int_{S_b^{(2)}} p^{(0)} \quad (4.27b)$$

The hydrostatic term in the pressure, $\rho g y$ is the buoyancy term. This is not taken into account for the hydrodynamic properties of the floating body. It does however become of importance with the equations of motion. For two dimensions, the equation becomes as shown below. This means for all linear equations only the 0-th order waterplane area is used. This approximates the sides of the body as straight lines. For a square, this is accurate. For a cylinder, it induces approximations.

$$\int_{S_b^{(0)}} \rho g \eta^{(1)} = \int_{S_a^{(0)}} \rho g (\eta^{(1)} - a^{(1)}) \quad (4.28a)$$

$$\int_{S_b^{(1)}} \rho g \eta^{(1)} = \int_{S_a^{(1)}} \rho g (\eta^{(1)} - a^{(1)}) \quad (4.28b)$$

4.4 Power prediction and optimal damping

The power can be predicted analytically to find the optimal damping of the PTO. To do this, the average power is determined and the optimal frequency is found. Then, for this frequency the optimal damping is determined. The power is known from the PTO characteristics as seen in Eq. (2.9), and is shown below:

$$P_d(t) = \lambda_{PTO} \dot{a}(t)^2 \quad (4.29)$$

The velocity is found from the oscillatory motion of the body, with \hat{a} the amplitude of the body motion. With the known velocity, the average power is calculated.

$$\dot{a}(t) = \omega \hat{a} \sin(\omega t) \quad (4.30a)$$

$$\dot{a}(t)^2 = \omega^2 \hat{a}^2 \sin^2(\omega t) \quad (4.30b)$$

With the following average power:

$$\bar{P}_d = \frac{1}{T} \int_0^T P_d(t) dt \quad (4.31a)$$

$$\bar{P}_d = \frac{1}{T} \int_0^T \lambda_{PTO} \omega^2 \hat{a}^2 \sin^2(\omega t) dt \quad (4.31b)$$

$$\bar{P}_d = \frac{1}{2} \lambda_{PTO} \omega^2 \hat{a}^2 \quad (4.31c)$$

The amplitude of the body is determined by the response amplitude operator (RAO, ζ_y). This is defined as the ratio between the incoming wave and body motions, for this case in heave: $\zeta_y = \hat{a}/A$. The expression for the RAO comes from an equation of motion with F_y the forces on the body in heave, the added mass μ , the damping coefficient λ and the buoyancy K . A new expression for the average power is found from there.

$$\zeta_y = \frac{F_y}{-\omega^2(M + \mu) - i\omega(\lambda + \lambda_{PTO}) + K} \quad (4.32a)$$

$$\bar{P}_d = \frac{1}{2} \lambda_{PTO} \omega^2 \zeta_y^2 A^2 \quad (4.32b)$$

$$\bar{P}_d = \frac{1}{2} \lambda_{PTO} \omega^2 \frac{F_y^2}{(K - \omega^2(M + \mu))^2 + (\omega(\lambda + \lambda_{PTO}))^2} A^2 \quad (4.32c)$$

$$\bar{P}_d = \frac{1}{2} \frac{\lambda_{PTO} \omega^2 A^2 F_y^2}{(K - \omega^2(M + \mu))^2 + (\omega(\lambda + \lambda_{PTO}))^2} \quad (4.32d)$$

With this expression for the average power, the optimal value for the optimal damping must be found. This is done by finding the derivative of the average power with regard to the PTO damping, and finding a root of this equation. This optimal damping will be used to find the power prediction of the floating body.

$$\frac{\partial \bar{P}_d}{\partial \lambda_{opt}} = 0 \quad (4.33a)$$

$$\frac{1}{2} \frac{\omega^2 \zeta_y^2 F_y^2 ((K - \omega^2(M + \mu))^2 + \omega^2(\lambda^2 - \lambda_{opt}^2))}{((K - \omega^2(M + \mu))^2 + (\omega(\lambda + \lambda_{opt}))^2)^2} = 0 \quad (4.33b)$$

$$\lambda_{opt} = \sqrt{(K/\omega - \omega(M + \mu))^2 + \lambda^2} \quad (4.33c)$$

4.5 Boundary Element Theory

An overview of a fluid domain is seen in Fig. 4.3. The sources have strengths which are found by solving for all boundary conditions.

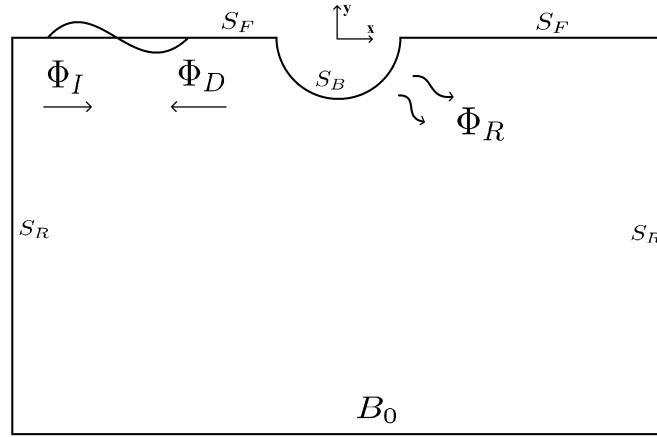


Figure 4.3: General overview of a domain of a 2D panel method

Abbreviation	Physical meaning
Φ_I	Incident wave
Φ_D	Diffracted wave
Φ_R	Radiated wave
S_B	Body surface
S_F	Free surface
S_R	Radiation boundary
B_0	Bottom boundary

Table 4.2: List of Abbreviations

Boundary Conditions Free Surface S_F

Both the linear kinematic and dynamic boundary conditions are applied to the surface. This can be combined to one single relation for all panels, the Haskind relation. Use is made of the oscillatory behaviour of the potential, meaning its time dependence is of $e^{i\omega t}$. This makes it simple to find the time derivative whilst remaining in the frequency domain. It should be noticed this boundary condition is of the mixed type, whereas the body boundary condition is a Neumann condition (Yeung, [31]). If no subscript is used, the condition holds for all different potentials.

$$\frac{\partial \eta}{\partial t} = \frac{\partial \Phi}{\partial y} \quad y = \eta \quad (4.34a)$$

$$\frac{\partial \Phi}{\partial t} + g\eta = 0 \quad (4.34b)$$

$$g \frac{\partial \Phi}{\partial y} = \frac{\partial^2 \Phi}{\partial t^2} \quad (4.34c)$$

$$\frac{\partial \Phi}{\partial y} + \frac{1}{g}(-i\omega)^2 \Phi = 0 \quad (4.34d)$$

$$\frac{\partial \Phi}{\partial y} - k\Phi = 0 \quad (4.34e)$$

The wave height can be found as below:

$$\eta = -\frac{1}{g} \frac{\partial \Phi}{\partial t} = \frac{-i\omega}{g} \Phi \quad (4.35)$$

Radiation Condition S_R

To prevent the necessity of modelling the free surface to infinity or implementing a numerical beach, a radiation condition is used. Boundary conditions on the edge of the fluid domain are used to simulate open boundaries. It is not desirable to have reflections of the outgoing waves to go back into the fluid domain. Waves created by the body must radiate away from the body (Bertram, [4]), with $\hat{\varphi}$ an undetermined constant amplitude and ω_e the encounter frequency of different waves:

$$\lim_{|x| \rightarrow \infty} (\Phi^D + \Phi^R) = Re\{\hat{\varphi} e^{ky} e^{i(kx - \omega_e t)}\} \quad (4.36)$$

For second order wave potentials, sum and difference frequency terms will also be present in the limit of the potential at infinity.

The Sommerfeld condition describes a boundary value that suppresses the reflected wave at the boundary. The condition that must be satisfied is seen in Eq. (4.37). This radiation condition is perfect for a two-dimensional problem. A Sommerfeld condition for bi-chromatic waves can be seen in Eq. (4.38).

$$\left(\frac{\partial}{\partial t} + c \frac{\partial}{\partial x} \right) \Phi^{(n)} = 0 \quad (4.37)$$

$$\left(\frac{\partial}{\partial t} + c_1 \frac{\partial}{\partial x} \right) \left(\frac{\partial}{\partial t} + c_2 \frac{\partial}{\partial x} \right) \Phi^{(n)} = 0 \quad (4.38)$$

Body surface S_B

At the body, the normal velocities have to be 0. This means the following no-penetration condition has to hold:

$$\frac{\partial \Phi^{(1)}}{\partial n_{S_B}} = 0 \quad (4.39)$$

Bottom boundary condition B_0

At the bottom, the normal velocities have to be 0. This means the following no-penetration condition has to hold:

$$\frac{\partial \Phi^{(1)}}{\partial n_{B_0}} = 0 \quad (4.40)$$

Infinite Depth

If the fluid is infinitely deep, the potential and velocities approach 0 as y approaches $-\infty$. As soon as the values approach infinitesimal values the boundary no longer has to be paneled. Also, as the magnitude of the potential and its derivative in y decreases, the spacing of the panels can increase. This is done with a logarithmic spacing function.

Chapter 5

Linear problem

In this chapter, only the linear problem with linear wave theory is regarded. A boundary element method is written to find the hydrodynamic properties of an arbitrary shape and to solve the complete system of motion with both the diffracted as the radiated waves. The choice is made for a method with simple sources instead of complicated Green functions, as this will be more suitable to extend to the second order problem. The linear problem is split in a diffraction and a radiation problem, which when coupled together give the complete motions of the cylinder. Additional information on a panel method is found in Appendix D.

5.1 Problem description

The resulting geometry (for few panels, to give an overview) is seen in Fig. 5.1. In this figure, all individual surfaces have only 5 panels for clarification purposes.

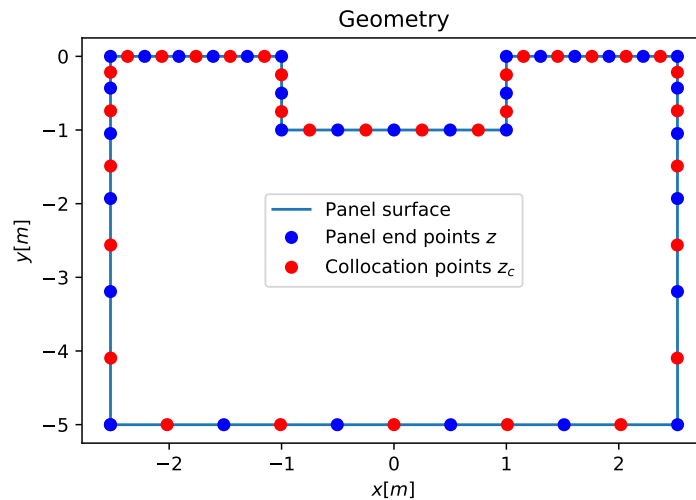


Figure 5.1: Panel Layout

The surfaces can be split in 6 different surfaces, similar to Fig. 4.3. The left radiation boundary (S_L , the left free surface S_F , the body surface S_B , the right free surface S_F , the right radiation boundary boundary S_R and the bottom boundary B_0 . These surfaces are subject to different boundary conditions, as shows in Section 4.5.

5.2 Boundary conditions

Free surface boundary condition

The conditions that have to be satisfied on the boundary are the kinematic boundary condition (which relates the height of the surface of the water to the particle velocities) and the dynamic boundary condition (no pressure jump since there is no surface tension). The boundary condition on the free surface is as follows:

$$\frac{\partial \Phi^{(1)}}{\partial y} - k \Phi^{(1)} = 0 \quad (5.1)$$

For a linear problem, the panels can simply be placed on $y = 0$. Using perturbation methods the boundary conditions can then be linearized around $y = 0$. Similarly to the body panels, these panels can be added to the influence matrix and solved for the boundary conditions. It is recommended to use at least 12 panels per wave length (Yeung, [31])

Body boundary condition

For the diffraction problem, the velocities normal to the body are 0. This is shown in the boundary condition below.

$$\frac{\partial \Phi^{(1)}}{\partial n_b} = 0 \quad (5.2)$$

For the radiation problem, the fluid velocities normal to the body must be equal to the normal velocities of the body surface. This will be the driving phenomena for the radiated waves.

$$\frac{\partial \Phi^{(1)}}{\partial n_b} = n_b \cdot \begin{bmatrix} 0 \\ 1 \end{bmatrix} \dot{\alpha}^{(1)}(t) \quad (5.3)$$

Bottom boundary condition

At the bottom boundary, the velocities normal to the bottom surface are 0.

$$\frac{\partial \Phi^{(1)}}{\partial n_{B_0}} = 0 \quad (5.4)$$

5.3 Generating absorbing boundary condition

A highlight of the thesis is the generation of waves on the radiation boundary, which interact with the body. To achieve this, the ABC for which the Sommerfeld condition is used, will be adapted to be a GABC.

The Sommerfeld condition is based on a propagating wave in a certain direction. On the left and right radiation boundaries, respectively right and left running waves are suppressed. This means no waves can reflect from the boundaries back into the domain, but waves exiting the domain can pass through freely.

$$\left(\frac{\partial}{\partial t} \pm c \frac{\partial}{\partial x} \right) \Phi^{(1)} = 0 \quad (5.5)$$

The wave speed is defined as ω/k for arbitrary depth. This means that for the frequency domain the equation simplifies to:

$$\left(\frac{\partial}{\partial x} \pm ik \right) \Phi^{(1)} = 0 \quad (5.6)$$

This Sommerfeld condition suppresses all waves in a chosen direction, depending on the chosen sign. This is also the expression used by Yeung [31] for his radiation problem.

For the diffraction problem, the right hand side of the equation must not be 0. There must be a right going wave at the left boundary, which is the incoming wave. Therefore, one right going wave is allowed by changing the right hand side of the equation from 0 to the incoming wave potential substituted in the Sommerfeld condition. This is done for finite volume problems in a time domain by Wellens [30]. The result for a single wave is seen in Fig. 5.2. The left boundary is a GABC, and the right boundary is an ABC. It can be seen the resulting numerical value is a near perfect match to the analytical potential.

$$\left(\frac{\partial}{\partial x} - ik\right)\Phi^{(1)} = \left(\frac{\partial}{\partial x} - ik\right)\Phi_I^{(1)} = -2ik\Phi_I^{(1)} \quad (5.7)$$

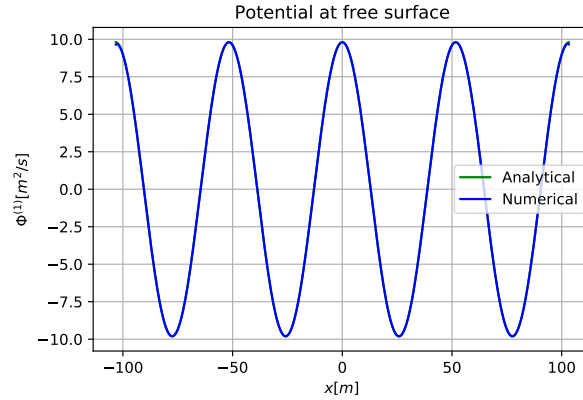


Figure 5.2: Right going wave potential

This boundary condition has proven to be accurate to generate a wave entering the domain, as will be seen in the results. For the right boundary, a ABC as shown in Eq. (5.6) is used. The spacing of the panels can increase with increasing depth, since the gradient of the potential decreases. This is done using a logarithmic spacing function.

5.4 Discretization

The approximate solution is achieved by solving a matrix equation, similar to the body boundary condition. since this is a mixed type boundary condition, the potential and the normal velocity must be defined on all panels. The condition is solved for each collocation point (observation point) on each respective panel. These are places just inside the fluid domain.

Source panels are used to find the solution to the boundary problem. These are sources spread out over the whole panel. More explanation is found in Chapter D. The influence matrix $P_{[m,n]}$ describes the influence of the potential of panel m on panel n. The influence matrix $Q_{[m,n]}$ is used to find the influence of panel m on panel n with regard to the normal velocity of the panel (pointing inwards of the fluid domain). Here, l is the panel length.

$$P_{[n,m]} = \int_{panel} \frac{l_{[n]}}{2\pi} \ln(z_{c[m]} - z_{1[n]}(s)) ds \quad (5.8a)$$

$$Q_{[n,m]} = \int_{panel} \frac{l_{[n]}}{2\pi} \frac{\partial}{\partial n_p} \ln(z_{c[m]} - z_{1[n]}(s)) ds \quad (5.8b)$$

$$z_1(s) = z_a + s(z_b - z_a) \quad (5.8c)$$

$$z = x + iy \quad (5.8d)$$

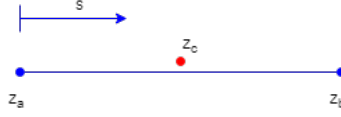


Figure 5.3: Panel Definitions

Implementation influence matrices

Implementing these influence matrices in a code is not a trivial task. A different approach is taken for the potential value influence matrix $P_{[m,n]}$ and the normal velocity influence matrix $Q_{[m,n]}$.

$P_{[m,n]}$ is found by numerical integration of sources along each panel. The challenge arises when $m = n$. At this panel, the collocation point z_c is very close to the panel surface. If the integration step is not small enough, integration errors will occur on this panel as the distance between the panel and collocation point is critical in the result. To ensure a good result, the integration step size has been reduced until the solution converges.

For $Q_{[m,n]}$, an analytical solution is found. The advantage of this solution is that it is faster to calculate the influence matrix than by doing a numerical integration. However, this computation time advantage is negligible compared to the computation time of matrix equation to find the source strengths. The analytical solution for $Q_{[m,n]}$ is seen in Eq. (5.9).

$$Q_{[m,n]} = Im \left\{ \sum_{n=1}^N \frac{1}{2\pi} \ln \left(\frac{z_c^{(m)} - z_a^{(n)}}{z_c^{(m)} - z_b^{(n)}} \right) \frac{ds}{dz_1} \Big|^{(n)} \frac{dz_1}{ds} \Big|^{(m)} \right\} \quad (5.9)$$

With these descriptions of the normal velocities and potential in the entire domain, the boundary conditions can be written in a discretized form. To solve for all boundaries simultaneously, the problem must be brought into one matrix equation.

$$C_{[n,m]}^{(1)} = \begin{cases} Q_{[n,m]} - i k P_{[n,m]} & , n \in S_L \\ Q_{[n,m]} & , n \in S_b \\ Q_{[n,m]} + k P_{[n,m]} & , n \in S_F \\ Q_{[n,m]} - i k P_{[n,m]} & , n \in S_R \\ Q_{[n,m]} & , n \in B_0 \end{cases} \quad (5.10)$$

This matrix C contains all influence matrices that need to be solved for. Another matrix, describing the known behaviour of the fluid at its boundaries is also determined. This matrix is different for the diffraction problem and the radiation problem.

Diffraction problem

$$K_{[n]}^{(1)} = \begin{cases} -2i k \Phi^{(1)} & , n \in S_L \\ 0 & , n \in S_b \\ 0 & , n \in S_F \\ 0 & , n \in S_R \\ 0 & , n \in B_0 \end{cases} \quad (5.11)$$

Radiation problem

$$K_{[n]}^{(1)} = \begin{cases} 0 & , n \in S_L \\ \dot{a}_{n[n]}^{(1)} & , n \in S_b \\ 0 & , n \in S_F \\ 0 & , n \in S_R \\ 0 & , n \in B_0 \end{cases} \quad (5.12)$$

with $\dot{a}_{n[n]}$ the normal body velocities

$$\dot{a}_{n[n]} = n_{b[n]} \cdot \mathbf{u}_{b[n]} \quad (5.13)$$

The source strengths $q_{[n]}$ can be found as a solution to the boundary problem.

$$C_{[n,m]}^{(1)} \cdot q_{[n]}^{(1)} = K_{[n]}^{(1)} \quad (5.14)$$

From this resulting source strength matrix the potential and free surface values can be found.

$$\Phi_{[n]}^{(1)} = q_{[n]}^{(1)} \cdot P_{[n,m]}^{(1)} \quad (5.15a)$$

$$\eta_{[n]}^{(1)} = \frac{-i\omega}{g} \Phi_{[n]}^{(1)} \quad n \in S_F \quad (5.15b)$$

5.5 Coupling radiation and diffraction problem

Combining the radiation and diffraction problem to find the power prediction and energy balance is a highlight of this thesis. The incoming wave induces forces on the cylinder, which causes the motions of the body. The body motions cause radiated waves away from the body and is solved separately, since the body motions are not known beforehand.

To find the energy balance of the complete system, these two problems need to be combined. This is done by finding the complex response amplitude operator (RAO) of the body. This has information on both the amplitude of the motion of the body and the phase difference to the incoming wave.

The diffraction force has components in phase with the potential and in phase with the velocities. The modulus of these components defines the amplitude of the force. In Fig. 5.11 the real part of the diffraction forces is in phase with the accelerations of the incoming wave. The imaginary part is in phase with the velocities of this wave. The combination of these creates a total phase difference with the incoming potential. This phase difference is dependent on the frequency.

$$F_y = \rho\omega \int_{S_b} (\varphi_2^{(n)} + i\varphi_1^{(n)}) \quad (5.16a)$$

$$F_y = |F_y| e^{i\omega t + \epsilon_y} \quad (5.16b)$$

The displacement and velocity of the body in the frequency domain is given as follows, with c_m a complex number for the amplitude and phase of the motion

$$a^{(1)}(t) = c_m^{(1)} e^{i\omega t} \quad (5.17a)$$

$$\dot{a}^{(1)}(t) = i\omega a^{(1)}(t) \quad (5.17b)$$

The motion amplitude and phase of the body will be defined by the complex RAO. The hydrodynamic coefficients in the definition of the RAO are determined from the radiation problem.

$$\zeta_y = \frac{F_y}{-\omega^2(M + \mu) - i\omega(\lambda + \lambda_{PTO}) + K} \quad (5.18a)$$

$$\zeta_y = |\zeta_y| e^{i\epsilon_\zeta} \quad (5.18b)$$

$$c_m^{(1)} = A |\zeta_y| e^{i\epsilon_\zeta} \quad (5.18c)$$

The real and imaginary parts of a can be written as the position and velocity of the body:

$$\alpha^{(1)}(t) = Re \{ a^{(1)}(t) \} \quad (5.19a)$$

$$\dot{\alpha}^{(1)}(t) = Re \{ i\omega a^{(1)}(t) \} \quad (5.19b)$$

With the correct phase difference and amplitude of the body the diffraction and radiation potentials can be added up to find the total potential. This allows for the calculation of energy conservation and finding the combined free surface elevation.

5.6 Validation and verification

To be able to use the model and expand it up to a second order panel method, the linear results must first be validated with proven models, or experimental results.

Diffraction problem

The results of the radiation coefficient are plotted in Section 5.6, for a square cylinder of $r_1 = r_2 = 1$. The infinite depth case compares quite well to the theoretical values of Ursell [26]. The experimental values from [16] differ from the numerical results from this method. This difference appears at higher frequencies, when the velocities are higher. This induces more viscous effects and non-linearity. Therefore, a difference between the experiments and BEM is most likely explained.

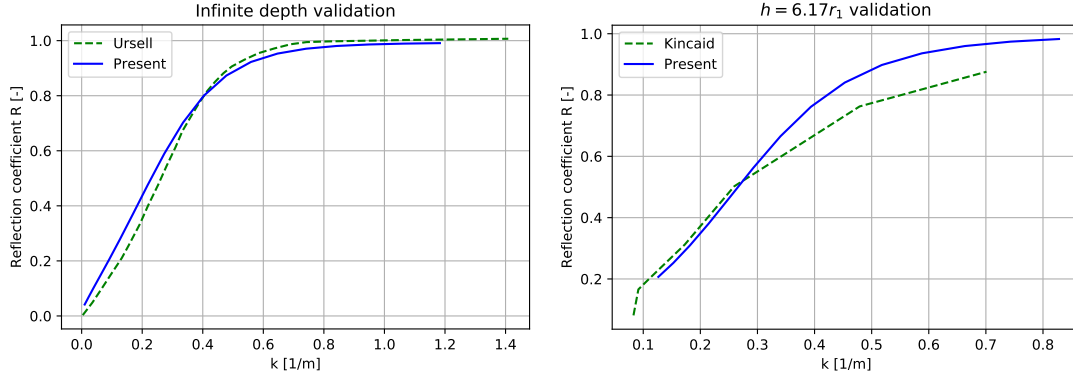


Figure 5.4: Reflection coefficient: Ursell's exact solution for infinite depth [26] and Kincaid's experiment for $h/r_1 = 6.17$ [16]

An error was found for the energy conservation. An analysis has been done to find the reason and the magnitude of these errors. It proved the grid size was not small enough to capture a linear propagating radiated wave. The radiated wave did not have a constant modulus, as would be expected from a linear wave. The resulting errors are seen below:

Table 5.1: Grid size errors

No. panels (side x surface x body)	Deviation in modulus η_L	$1 - (R^2 + T^2)$
30x60x60	17.1 %	0.058
50x100x60	11.4 %	0.037
100x200x90	7.0 %	0.021
200x400x120	4.8 %	0.011

Radiation problem

The radiation problem can be validated with the results from Yeung [31]. Yeung published results for circular cylinders, which should be identical.

The found values from the panels method are compared with the results from Yeung for two frequencies, with the following condition: wave number $k = \frac{\omega^2}{g} r$ (a difference is seen in the non-finite depth of Yeung's method). The chosen values for k are 1.5 and 0.9. The comparison between the values of the potential at the body surface are seen in Fig. 5.5. It can be seen there is almost no difference between the results.

A comparison with the added mass and damping forces with the panel method by Frank [9], which used a complicated green function for the free surface boundary conditions for infinite depth, is seen in Fig. 5.6. What can be seen is that the added mass terms of the current method are higher than the comparisons. At

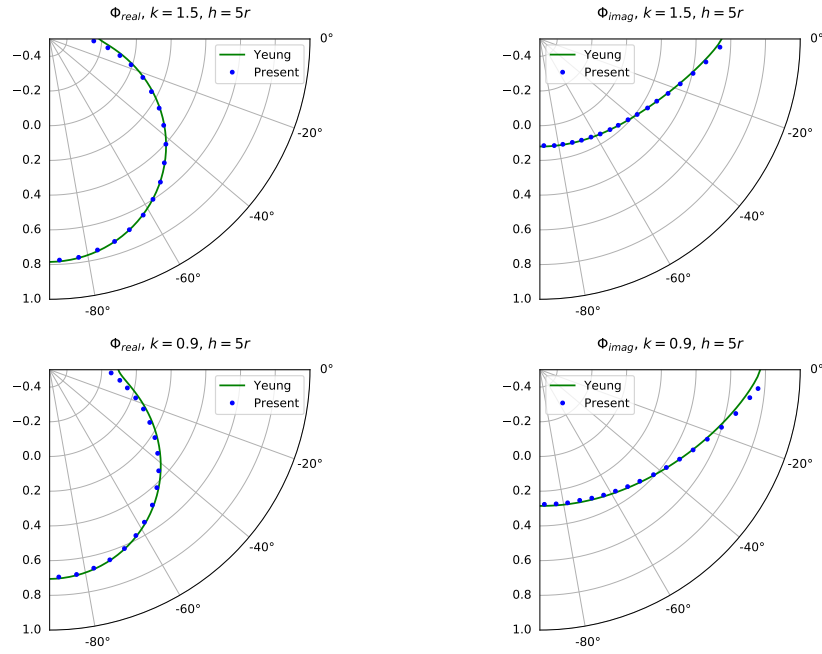


Figure 5.5: Potential value comparison Yeung [31]

larger frequencies these differences disappear. The coefficients are made non-dimensional as seen below

$$\mu_{nd} = \frac{\mu}{0.5 \pi r^2} \quad (5.20a)$$

$$\lambda_{nd} = \frac{\lambda}{0.5 \pi \omega r^2} \quad (5.20b)$$

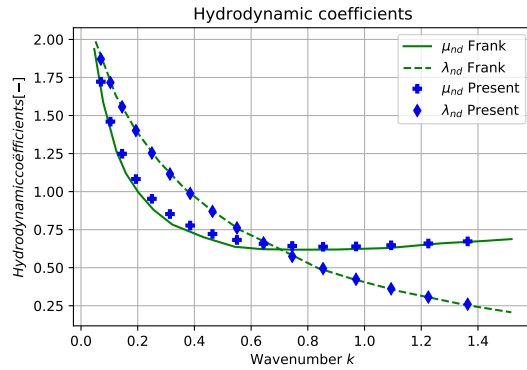


Figure 5.6: Validation hydrodynamic coefficients

RAO

The amplitude of the RAO is a combination of the diffraction and radiation problem. This has been validated with the numerical results from Isaacson et al. [11] and the analytical results from Zhao et al. [32]. Their results are for a finite depth of $h = 5r_2$, which should only give very small deviations from infinite depth. The result is seen in the figure below, Fig. 5.7, for a square with a ratio $r_1/r_2 = 1.5$.

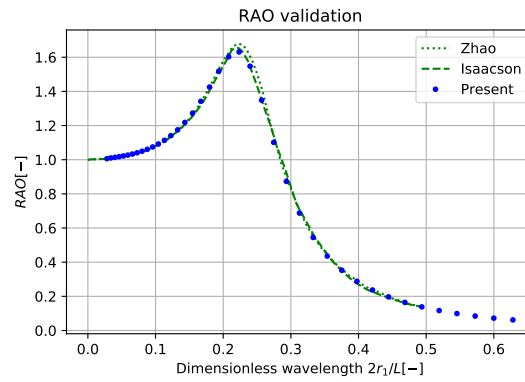


Figure 5.7: RAO validation

Radiation boundary convergence

In order to achieve a solution with only propagating waves leaving the domain, there must be no effect of the evanescent waves at the position of the radiation condition. According to theory, a few wavelengths should be sufficient to find a converging solution. For the current method, several boundary positions are plotted to see what distance is required. For the comparison, $k = 0.1$ and $r = 1$ is chosen.

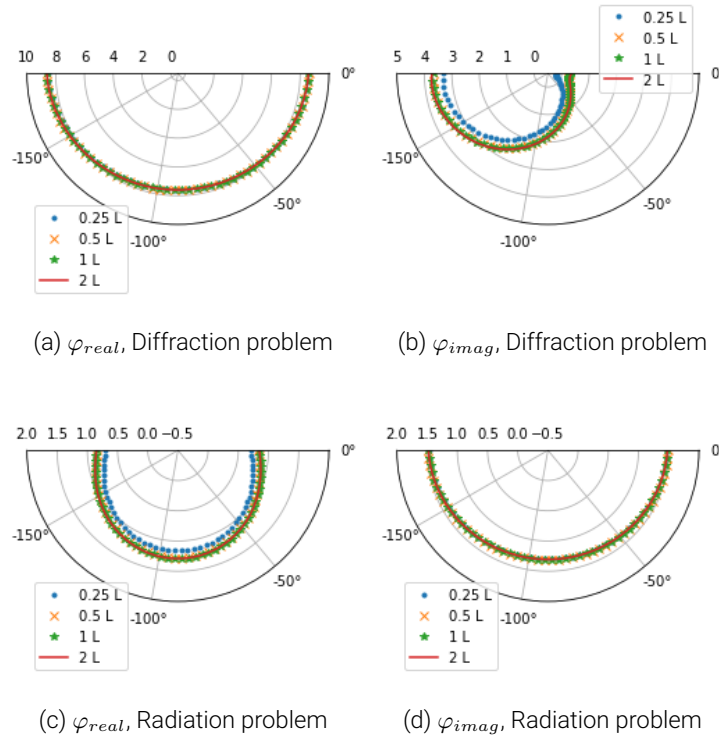


Figure 5.8: Radiation boundary convergence

It can be seen the value already looks converged at 0.5 wavelengths away from the body. This shows the 2 wavelengths used for the solutions is at a sufficient distance.

5.7 Results

The results are shown in this section. First, the diffraction problem is solved, then the radiation problem. These are then coupled to find the total forces and motions of the floating body. Also, a power take off is included in the system. An overview of the resulting wave profiles is seen in Fig. 5.9. In the diffraction problem, at the left side of the body a partly propagating wave is seen. It is a combination of the incoming wave and the reflected wave from the body. At the right side of the body, the transient wave is seen. This is a propagating wave to the right side. In the radiation problem, a left running wave is seen at the left of the body and a right running wave at the right of the body. These both propagate away from the body. The combined solution for a free floating cylinder and with PTO is seen in Fig. 5.10.

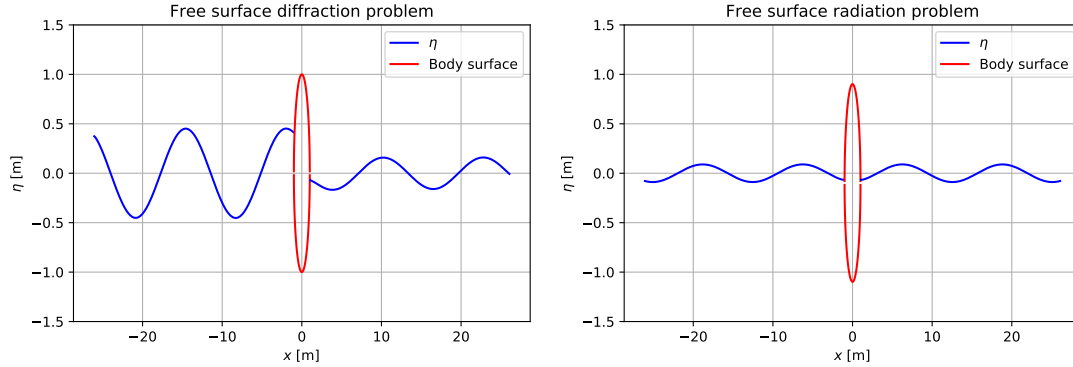


Figure 5.9: Wave profiles with body

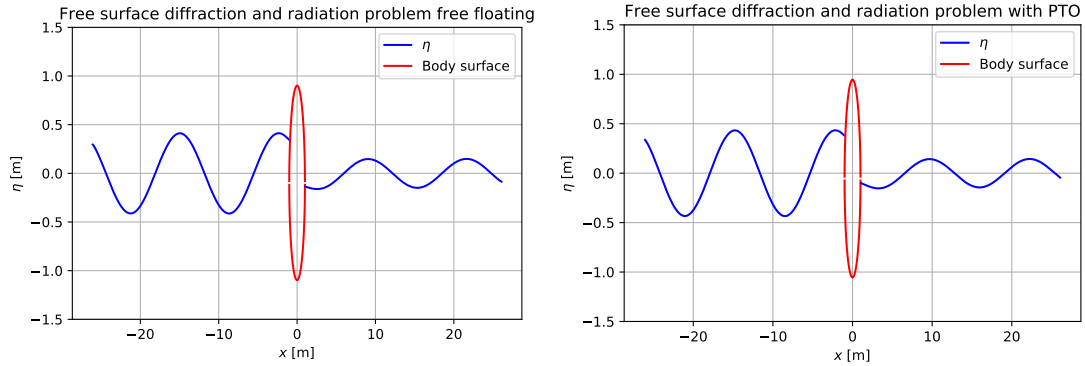


Figure 5.10: Wave profiles with body combined

Diffraction Forces

The cylinder is in motion due to the forces found from the diffraction problem. As shown in Section 4.3, the linearized Bernoulli equation, the pressures are found (Eq. (5.21)). To find the hydrodynamic behaviour, the hydrostatic pressures $\rho g y$ are not regarded to find the hydrodynamic pressures. As shown by Zhao et al. [32], the heaving force is found as seen in Eq. (5.22). This equation shows the time derivative of the incoming and diffracted potential.

$$p = \rho \frac{\partial \Phi}{\partial t} + \rho g y \quad (5.21)$$

$$F_y = \rho i \omega \int_{S_b} (\Phi_I + \Phi_D) ds \quad (5.22)$$

The potential found from the panel method is split in a space- and time-dependent part. This is done as

below:

$$\Phi^{(n)}(x, y, t) = \Phi_1^{(n)} + i\Phi_2^{(n)} \quad (5.23a)$$

$$= \varphi^{(n)}(x, y) \cdot e^{i\omega t} \quad (5.23b)$$

$$\varphi^{(n)}(x, y) = \varphi_1^{(n)} + i\varphi_2^{(n)} \quad (5.23c)$$

$$\Phi^{(n)} = \varphi_1^{(n)} e^{i\omega t} + i\varphi_2^{(n)} e^{i\omega t} \quad (5.23d)$$

This is substituted in Eq. (5.22), resulting in the following discretized expression for the heaving force:

$$|F_y| = \rho\omega \sum_{n=1}^{N2:N3} (\varphi_2^{(n)} + i\varphi_1^{(n)}) \quad (5.24a)$$

$$F_y = |F_y| e^{i\omega t + \epsilon_y} \quad (5.24b)$$

The force has components in phase with the potential and in phase with the velocities. The modulus of these components defines the amplitude of the force. In Fig. 5.11 the real part of the diffraction forces is in phase with the accelerations of the incoming wave. The imaginary part is in phase with the velocities of this wave. The combination of these creates a total phase difference with the incoming potential. This phase difference is dependent on the frequency. The results of the force amplitude and phase difference is seen in Fig. 5.11. At low frequencies, the forces are almost exclusively in phase with the accelerations of the incoming wave, meaning the cylinder will almost exactly move along with the free surface.

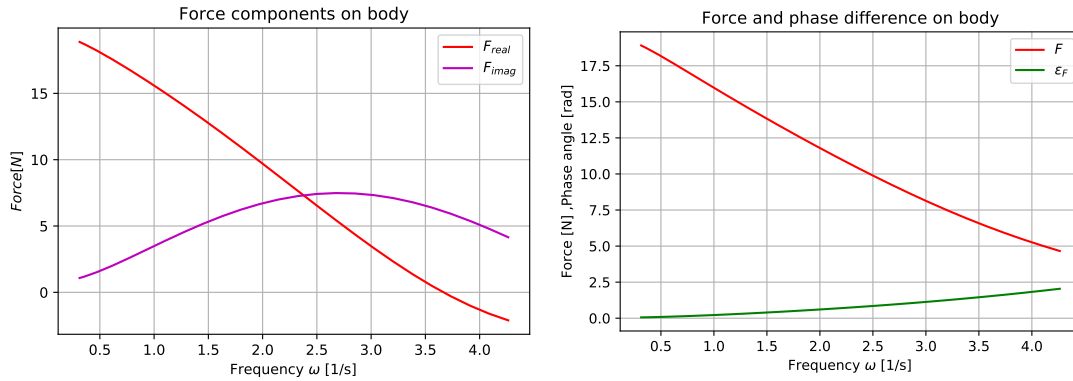


Figure 5.11: Diffraction forces on a cylinder in heave

Radiation Forces

First, the values of the only space-dependent potential (φ) have to be found. The potential found from the panel method is complex in both space and time, with parts in phase with the velocity and with the displacement.

$$\Phi^{(n)}(x, y, t) = \Phi_1^{(n)} + i\Phi_2^{(n)} \quad (5.25a)$$

$$= \varphi^{(n)}(x, y) \cdot \dot{\alpha}(t) \quad (5.25b)$$

$$\varphi^{(n)}(x, y) = \varphi_1^{(n)} + i\varphi_2^{(n)} \quad (5.25c)$$

$$\Phi^{(n)} = \varphi_1^{(n)} \cdot \dot{\alpha}(t) + \omega \varphi_2^{(n)} \alpha(t) \quad (5.25d)$$

As expected, the time-independent values for φ do not change when the phase of the motion is changed.

With the Bernoulli equation the dynamic pressures on the body can be calculated. The hydrostatic pressures also vary in time due to the free surface elevation, but this is not taken into account here. The second

order effect of the pressure is neglected here. With these dynamic pressures the added mass μ and damping coefficient λ are found, where the added mass is in phase with the accelerations and the damping in phase with the velocity. The resulting coefficients for a cylinder in heave is seen in Fig. 5.12.

$$F = \int_{S_b} p \cdot n_b ds \quad (5.26a)$$

$$F = \sum_{n=1}^{N2:N3} -\rho (\varphi_1^{(n)} \cdot n_b) \ddot{\alpha}(t) - \rho \omega (\varphi_2^{(n)} \cdot n_b) \dot{\alpha}(t) \quad (5.26b)$$

$$F = -\mu \ddot{\alpha}(t) - \lambda \dot{\alpha}(t) \quad (5.26c)$$

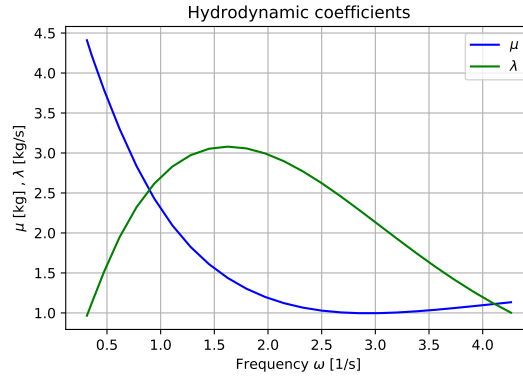


Figure 5.12: μ and λ for a cylinder in heave

Equations of motion

The resulting RAO of the cylinder in heave can be found with the following equation, where K is the spring term from the buoyancy force (Zhao et al. [32]). This approximates the walls of the body as straight lines, as explained in Section 4.3.

$$\zeta_y = \frac{F_y}{-\omega^2(M + \mu) - i\omega(\lambda + \lambda_{PTO}) + K} \quad (5.27)$$

An optional power take off damping is included, which if set to zero represents the free floating cylinder. K is the spring stiffness, which is represented by the buoyancy ($K = 2r\rho g$). This term shows only the buoyancy that occurs on top of the buoyancy at the position of the cylinder at rest, where the buoyancy and weight cancel each other. The resulting RAO in heave for a free floating cylinder can be seen in Fig. 5.13. At low frequencies the RAO is 1, which means the motions are equal to the wave elevation. This is as expected, since the spring term (buoyancy) is dominant for low frequencies. A peak in the RAO appears around the natural frequency. The motions in this area are dominated by damping effects. Finally, for very large frequencies the RAO approaches zero. This is because the inertia forces from the mass and added mass of the floating body are dominant, and the floating body will barely move.

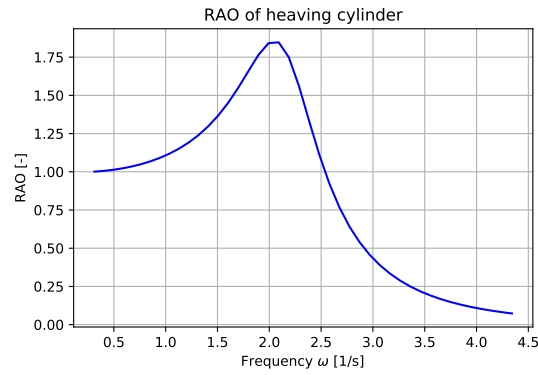


Figure 5.13: RAO of a cylinder in heave

Power prediction

As seen in Section 4.4 the optimal PTO damping is defined as $\lambda_{opt} = \sqrt{(K/\omega - \omega(M + \mu))^2 + \lambda^2}$. The incoming wave power and absorbed power are seen below. Note that from Fig. 2.1, only the damping term contributes to the absorbed power and will therefore be evaluated. A WEC with this damping is called ideally damped.

$$P_I = \frac{1}{2} \frac{\rho g A^2 \omega}{k} \quad (5.28a)$$

$$P_A = \frac{1}{2} \lambda_{PTO} \omega^2 \zeta_y^2 \quad (5.28b)$$

With these parameters the hydrodynamic efficiency of the wave energy converter can be calculated:

$$\eta_h = \frac{P_A}{P_I} \quad (5.29)$$

The results for the damped system are seen in Fig. 5.14. It can be seen the largest hydrodynamic efficiency is found around the natural frequency, with a value of around 50%.

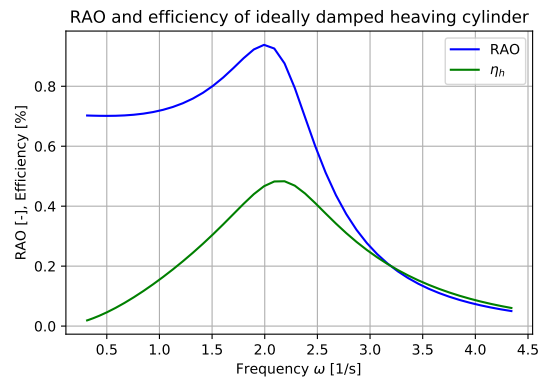


Figure 5.14: RAO and efficiency of ideally damped heaving cylinder

Energy conservation

The energy flux entering the domain should be equal to the energy flux leaving the domain. For a fixed body, the only energy entering the domain is the incident wave, and the energy leaving the body is the radiated and transient wave. Conservation of energy is then described as in Eq. (5.31).

Transmission and reflection coefficients are used to show the effect of the body on the waves. They are

the ratio of amplitudes of the reflected and transmitted wave to the incident wave. The behaviour with a square cylinder (square = cross section in x-y plane, cylinder = infinitely long floating object) can be seen in Fig. 5.15. The incident wave is subtracted from the reflected wave, as the amplitude of the standing wave is the sum of both waves. The wave heights are calculated sufficiently away from the body, to prevent any influence of the evanescent waves.

$$R = \frac{\eta_L}{A} = \frac{\Phi_D}{\Phi_I} \quad x = x_L \quad (5.30a)$$

$$T = \frac{\eta_R}{A} = \frac{\Phi_D + \Phi_I}{\Phi_I} \quad x = x_R \quad (5.30b)$$

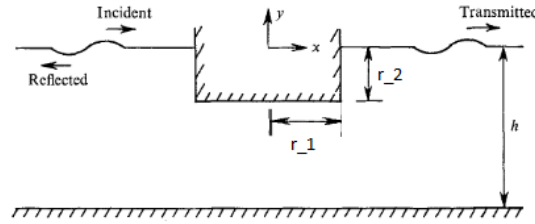


Figure 5.15: Wave definitions [20]

$$P_I = P_R + P_T \quad (5.31a)$$

$$\frac{1}{2} \frac{\rho g A^2 \omega}{k} = \frac{1}{2} \frac{\rho g \eta_L^2 \omega}{k} + \frac{1}{2} \frac{\rho g \eta_R^2 \omega}{k} \quad (5.31b)$$

$$A^2 = \eta_L^2 + \eta_R^2 \quad (5.31c)$$

$$R^2 + T^2 = 1 \quad (5.31d)$$

The results of these equations are plotted below in Fig. 5.16.

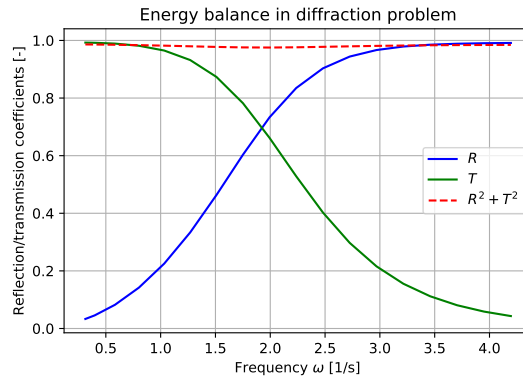


Figure 5.16: Radiation and Transmission coefficients and Energy conservation

For a problem with a moving body and power take off, it is slightly different. The radiated wave from the moving body and the power extracted by the PTO become part of the energy losses in the domain. The resulting equations are seen below. The resulting energy conservation is seen in Fig. 5.17. The derivation of the energy conservation is given in Eq. (5.33), as performed by Zhao et. al.[32], who used an analytical model of a floating square to find these results. Here, η_L and η_R are respectively the wave heights at the left and right of the body. η_h is the hydrodynamic efficiency.

$$R = \frac{\Phi_D - \zeta_y \Phi_R}{\Phi_I} \quad (5.32a)$$

$$T = \frac{\Phi_D + \Phi_I - \zeta_y \Phi_R}{\Phi_I} \quad (5.32b)$$

$$R^2 + T^2 + \eta_h = 1 \quad (5.32c)$$

$$P_I = P_R + P_T + P_A \quad (5.33a)$$

$$\frac{1}{2} \frac{\rho g A^2 \omega}{k} = \frac{1}{2} \frac{\rho g \eta_L^2 \omega}{k} + \frac{1}{2} \frac{\rho g \eta_R^2 \omega}{k} + \eta_h P_I \quad (5.33b)$$

$$A^2 = \eta_L^2 + \eta_R^2 + A^2 \eta_h \quad (5.33c)$$

$$R^2 + T^2 + \eta_h = 1 \quad (5.33d)$$

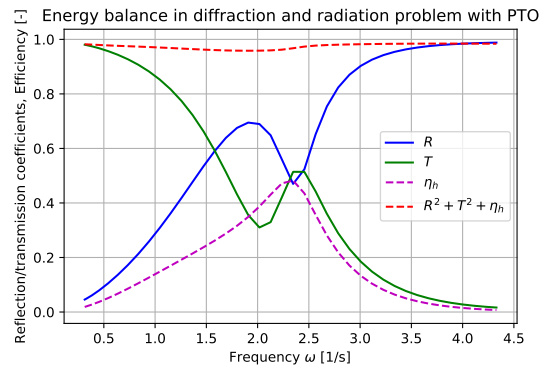


Figure 5.17: Energy conservation with PTO

Errors radiation boundary and free surface

The values of the velocities at the free surface boundary close to the radiation boundary, and at the radiation boundary close to the free surface boundary, show some errors. The values directly prescribed by the boundary conditions seem to be calculated correctly. However, the tangential components on the panels show some errors. These are difficult to explain, since the perfect analytical solution is a solution to all boundary conditions. When this ideal solution is prescribed, all sources go to 0. This means the perfect analytical solution is indeed a solution to the boundary conditions. If these errors are excluded in the relevant equations, it does not provide a significant problem. The presented comparison in Fig. 5.18 and Fig. 5.19 are done for a domain without body, so it can be compared to the theoretical values. It can be seen close to the boundary intersections the velocities deviate from the analytical solution.

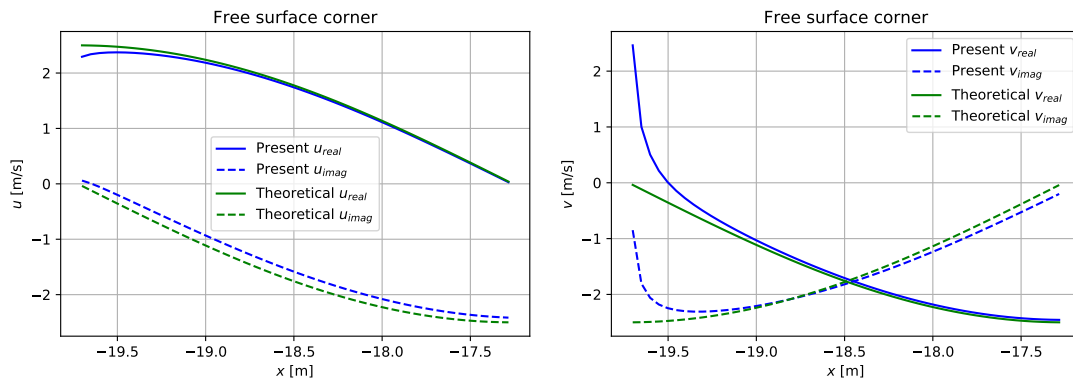


Figure 5.18: Corner problem at free surface

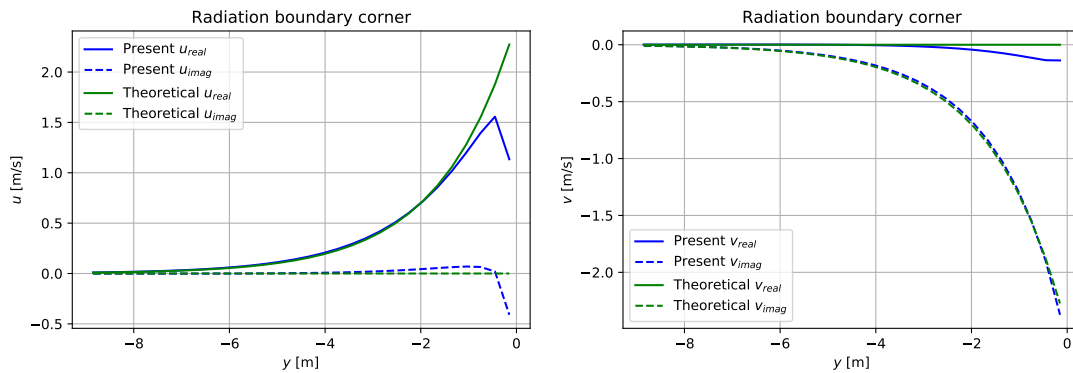


Figure 5.19: Corner problem at radiation boundary

5.8 Conclusions

It can be concluded that the first order method has been developed successfully. the goal was to develop a linear panel method for a cylinder oscillating on the free surface with a power take off.

Boundary conditions

The boundary conditions applied in the method are validated. The free surface boundary condition is derived from the pressure- and kinematic conditions at the free surface. This boundary condition is based on physics and is implemented correctly. The body and bottom boundary no-penetration boundaries are also modelled correctly. Finally, the GABC and ABC at the left and right radiation boundaries function well.

Some errors appear in close proximity of the intersection point between the free surface and radiation boundaries, but these are very local. The results have been validated despite these errors. Also, the expected behaviour of linear propagating waves at the boundaries is not perfect. Some non-linearity arises in the form of a non-constant amplitude of the reflected wave. This is due to a discretization error, as the error reduces significantly for smaller panels.

The evanescent waves appear not to be significant to the solution if the radiation boundary is placed 0.5 wavelengths away from the body. This is for a linear wave, for a non-linear wave the behaviour should be re-evaluated.

Geometries

Different geometries are validated in this linear method. This leads to the founded expectation that other geometries can be used in this method with success.

Energy balance

The diffraction problem successfully abides the energy conservation laws. This shows the coupling between the diffraction and radiation problem was successful, and the energy prediction of the PTO predicts the same amount of energy that is lost from the waves.

Chapter 6

Second order problem

This chapter describes the second order problem. The problem is split in a diffraction and radiation problem. Unlike the linear model, these can not simply be superimposed to find the complete motion of the object, since there is a non-linear interaction between the waves. This can be overcome by solving the radiation and diffraction problem simultaneously and adding coupling terms.

The second order problem has not been completely solved in this report. This chapter will present the model as developed, and will discuss the obtained results. The model can currently run a monochromatic wave through the finite depth domain, without interference with a body.

Problem definition

The same geometry is used as for the linear problem, as seen in Fig. 5.1. The same distinction between the surfaces is made.

6.1 Non-linear model

This section shows the theoretical model for a second order problem. The boundary conditions and discretization steps are displayed. The problem is no longer linear and the choice is made to keep the panels at the same locations. Second order effects are included through both the inclusion of non-linear terms in the boundary conditions and through Taylor expansions around the existing panel surfaces. This means the problem is still described as a single matrix equation to solve for the source strengths.

6.1.a Boundary conditions

Free surface boundary condition

The free surface boundary condition for second order can be seen in Eq. (4.15d). The panels are placed at $y = 0$, as the boundary condition is a Taylor expansion around $y = 0$. This right hand side is commonly called the quadratic forcing function [14]. The details of this derivation are found in Appendix C.

$$-4\omega\Phi^{(2)} + g\frac{\partial\Phi^{(2)}}{\partial y} = -\frac{\partial}{\partial t}\left(\frac{\partial\Phi^{(1)}}{\partial x}\frac{\partial\Phi^{(1)}}{\partial x} + \frac{\partial\Phi^{(1)}}{\partial y}\frac{\partial\Phi^{(1)}}{\partial y}\right) + \frac{1}{g}\frac{\partial\Phi^{(1)}}{\partial t}\frac{\partial}{\partial y}\left(\frac{\partial^2\Phi^{(1)}}{\partial t^2} + g\frac{\partial\Phi^{(1)}}{\partial y}\right) \quad (6.1)$$

$$Q_{FF} = -\frac{\partial}{\partial t}\left(\frac{\partial\Phi^{(1)}}{\partial x}\frac{\partial\Phi^{(1)}}{\partial x} + \frac{\partial\Phi^{(1)}}{\partial y}\frac{\partial\Phi^{(1)}}{\partial y}\right) + \frac{1}{g}\frac{\partial\Phi^{(1)}}{\partial t}\frac{\partial}{\partial y}\left(\frac{\partial^2\Phi^{(1)}}{\partial t^2} + g\frac{\partial\Phi^{(1)}}{\partial y}\right) \quad (6.2)$$

Left radiation boundary condition

The second order term of the incoming wave is the only right going second order locked wave at the left boundary. Therefore the Sommerfeld condition will again be used as a GABC. Note that the wave speed is the same wave speed as for the linear wave, since it is a locked wave.

$$\left(\frac{\partial}{\partial x} - 2ik\right)\Phi^{(2)} = \left(\frac{\partial}{\partial x} - 2ik\right)\Phi_I^{(2)} = -4ik\Phi_I^{(2)} \quad (6.3)$$

This no longer works when the pressure term from Eq. (4.21) or Eq. (4.22) appear. The additional pressure term will have an influence on the time derivative part of the potential, but the spacial derivative is 0. Since the Sommerfeld equation is based on propagating waves, this is no longer valid.

Possibly the Sommerfeld condition is not required at all. The second order potential is a function dependent on the first order potential, which is already successfully generated at the boundary. Therefore the second order wave is also created without the necessity to generate it at the boundary.

Right radiation boundary condition

The right radiation boundary is as follows, with the same exceptions as stated above.

$$\left(\frac{\partial}{\partial x} + 2ik\right)\Phi^{(2)} = 0 \quad (6.4)$$

Body surface

At the body surface, the velocities normal to the body must be 0 for the diffraction problem.

$$\frac{\partial\Phi^{(2)}}{\partial n_b} = 0 \quad (6.5)$$

For the radiation problem, they must be equal to the second order component of the velocity of the body.

$$\frac{\partial\Phi^{(2)}}{\partial n_b} = \dot{a}_N^{(2)}(t) \quad (6.6)$$

Bottom boundary condition

At the bottom surface, the no-penetration boundary condition holds.

$$\frac{\partial\Phi^{(2)}}{\partial n_{B_0}} = 0 \quad (6.7)$$

6.1.b Discretization

This section is split in two parts. First, the model with Sommerfeld condition with the same matrices as the linear problem is presented. This method is not yet fully functional, as will be discussed with the results. Secondly, a working model for a running wave without body is presented. This uses a new matrix that replaces the $Q_{[n,m]}$ matrix to find the velocities at the free surface.

Model 1

Similar to the first order solution, a matrix equation is solved containing all boundary conditions and wave parameters. The $P_{[n,m]}$ and $Q_{[n,m]}$ influence matrices are unchanged from the linear problem. The matrix containing all boundary condition components of the second order potential is seen below. This $C_{[n,m]}^{(2)*}$ matrix contains the Sommerfeld condition to generate the second order wave and uses the $Q_{[n,m]}$ matrix to find the normal velocities on the panels.

$$C_{[n,m]}^{(2)*} = \begin{cases} Q_{[n,m]} - 2i k P_{[n,m]} & , n \in S_L \\ Q_{[n,m]} & , n \in S_b \\ Q_{[n,m]} + 4k P_{[n,m]} & , n \in S_F \\ Q_{[n,m]} - 2i k P_{[n,m]} & , n \in S_R \\ Q_{[n,m]} & , n \in B_0 \end{cases} \quad (6.8)$$

The equations on the right hand side are less trivial than the linear problem, since the right hand side of the free surface is not zero but instead the QFF.

Diffraction problem

$$K_{[n]}^{(2)*} = \begin{cases} \left(\frac{\partial}{\partial x} - 2ik \right) \Phi_I^{(2)} & , n \in S_L \\ 0 & , n \in S_b \\ QFF_{[n]} & , n \in S_F \\ 0 & , n \in S_R \\ 0 & , n \in B_0 \end{cases} \quad (6.9)$$

Radiation problem

$$K_{[n]}^{(2)*} = \begin{cases} 0 & , n \in S_L \\ \dot{a}_N^{(2)}(t) & , n \in S_b \\ QFF_{[n]} & , n \in S_F \\ 0 & , n \in S_R \\ 0 & , n \in B_0 \end{cases} \quad (6.10)$$

Model 2

Another matrix is created which does not use the Sommerfeld condition to generate the second order wave and which does not use the $Q_{[n,m]}$ matrix, but instead the $G_{[n,m]}$ matrix as defined in Eq. (6.11).

$$G_{[n,m]} = \frac{\partial}{\partial y} P_{[n,m]} = 2k \tanh(2k(h+y)) P_{[n,m]} \quad (6.11)$$

The $\tanh(2k(h+y))$ term originates from the transformation of the $\cosh(2k(h+y))$ to a $\sinh(2k(h+y))$ when taking the partial derivative in y . This matrix can only be used for a running wave without a body, because of this use of the derivative.

$$C_{[n,m]}^{(2)} = \begin{cases} g G_{[n,m]} - 4\omega^2 P_{[n,m]} & , n \in S_F \\ G_{[n,m]} & , n \in B_0 \end{cases} \quad (6.12)$$

Since there is no body, only one right hand side is necessary.

$$K_{[n]}^{(2)} = \begin{cases} QFF_{[n]} & , n \in S_F \\ 0 & , n \in B_0 \end{cases} \quad (6.13)$$

6.2 Results

The goal of this chapter is to clearly communicate the possibilities and challenges of the linear model with regard to the second problem, and to increase the understanding of the second order problem to the reader. For all results, the following values are used: $A = 1[m]$, $\omega = 1[1/s]$, $h = 10[m]$. The second order potential found is seen in Eq. (6.14).

$$\Phi^{(2)} = \frac{3A^2\omega}{8} \frac{\cosh(2k(h+y))}{\sinh^4(kh)} e^{-2ikx} e^{2i\omega t} \quad (6.14)$$

Radiation boundary condition

Since the problem is a two-dimensional wave, the Sommerfeld condition will work without errors as a generating absorbing boundary condition. In this boundary condition it is important to note that the wave speed is the same speed as the first order wave, since it is a locked wave and the dispersion relation is not valid for the properties of that wave.

The results of the potential on the radiation boundary is seen in Fig. 6.1. To ensure the boundary is tested properly, the theoretical potential value is prescribed as a boundary condition on the free surface. This leaves the radiation boundary condition to be evaluated. It can be seen that it is nearly a perfect fit. The differences can most likely be explained as discretization errors.

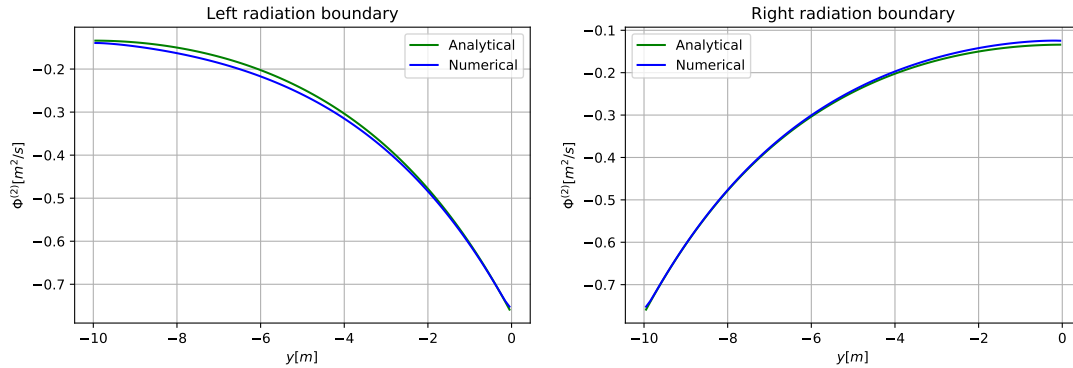


Figure 6.1: Radiation boundaries

However, as described, the Sommerfeld condition may not be necessary to obtain the correct second order wave.

Free surface boundary condition

To solve the free surface boundary condition, first the quadratic forcing function needs to be found. The quadratic forcing function is calculated as seen in Eq. (6.2). To find the values numerically, some challenges arise. Two components need to be found that are not present in the first order problem and existing model.

Firstly, the $\nabla\Phi^{(1)}$ term requires the tangential component of the flow along the panels. This can be found from the original velocity influence matrix. As shown in the appendix in Chapter D, the velocity influence matrix $V_{[n,m]}$ has a real and imaginary part. In Eq. (D.12), it is shown the tangential velocity is found from the real part of the velocity influence matrix. This is what we now define as $Q_{t[n,m]}$, with t_p the tangential unit vector of the panels.

$$Q_{t[n,m]} = \int_{panel} \frac{l_{[n]}}{2\pi} \frac{\partial}{\partial t_p} \ln(z_{c[m]} - z_{1[n]}(s)) ds \quad (6.15)$$

When discretized, it results in the following equation for the tangential flow at the free surface

$$\frac{\partial}{\partial x} \Phi^{(1)} = q_{[n]}^{(1)} \cdot Q_{t[n,m]} \mid n \in S_F \quad (6.16)$$

Secondly, the $\frac{\partial^2}{\partial y^2}$ of the potential has to be found. For the propagating waves, this is found as seen below:

$$\frac{\partial^2}{\partial y^2} \Phi^{(1)} = k^2 \Phi^{(1)} \quad (6.17)$$

However, as seen in Eq. (6.18) by Mei [19] for a Green function, the evanescent waves are of different nature. The behaviour in y direction is not a hyperbolic cosine but a normal cosine. This means the double derivative in y would result in $-k^2 \Phi^{(1)}$. Therefore, Eq. (6.17) can not be used to find the double derivative. This would result in errors close to the body where evanescent waves appear. This is where the results are most critical to determine the hydrodynamic properties of the floating object.

$$G = -\frac{i}{k} \left(h + \frac{1}{\sigma} \sinh^2 kh \right)^{-1} e^{ik|x-x_0|} \cosh(k(z+h)) \cosh(k(z_0+h)) \\ + \sum_{n=1}^{\infty} \frac{1}{k_n} \left(h + \frac{1}{\sigma} \sinh^2 k_n h \right)^{-1} e^{-k_n|x-x_0|} \cos(k_n(z+h)) \cos(k_n(z_0+h))$$

A different approach is taken. since the velocities inside the fluid can be determined at any point, a numerical differentiation is done very close to the free surface. A differentiation step is shown in Eq. (6.19), with ϵ a very small number. Ideally, the differentiation would be done between $y = \epsilon$ and $y = -\epsilon$ to find the value at $y = 0$. However, above $y = 0$ but below the panels the singularities and numerical integration at the panels make the solutions less accurate. Above the panels the result is no longer physical, since the velocities are not continuous when crossing a panel.

$$\frac{\partial^2}{\partial y^2} \Phi^{(1)} \Big|_{y=0} \approx \frac{\frac{\partial}{\partial y} \Phi^{(1)} \Big|_{y=0} - \frac{\partial}{\partial y} \Phi^{(1)} \Big|_{y=-\epsilon}}{\epsilon} \quad (6.19)$$

The result is seen in Fig. 6.2, comparing the found values for a propagating wave only. It compares the analytical solution to the numerical differentiation. Since it is only a propagating wave, Eq. (6.17) can also be used to find the accelerations at the free surface. The results show the values are nearly identical. Some errors occur close to the radiation boundary, which is not related to this problem.

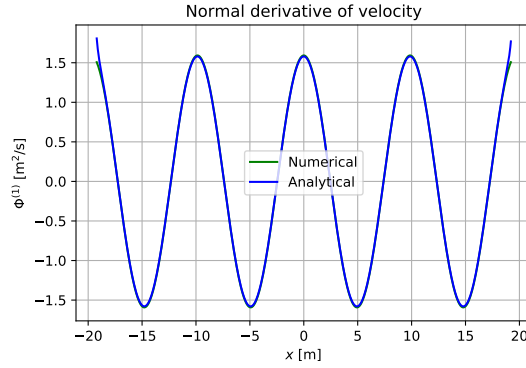


Figure 6.2: Normal derivative velocity on the free surface

The quadratic forcing function on the free surface is then determined as follows. It is important to note that the square of a complex number is not the same as the square of a cosine. Therefore the square has to be taken as seen in Eq. (6.21). The mean terms originating from the square of the complex numbers disappear when taking the derivative in time.

$$\frac{\partial}{\partial y} \Phi_{[n]}^{(1)} = q_{[n]}^{(1)} \cdot Q_{[n,m]} \quad (6.20a)$$

$$\frac{\partial}{\partial x} \Phi_{[n]}^{(1)} = q_{[n]}^{(1)} \cdot Q_{t[n,m]} \quad (6.20b)$$

$$\frac{\partial^2}{\partial y^2} \Phi_{[n]}^{(1)} = \frac{\frac{\partial}{\partial y} \Phi_{[n]}^{(1)} \Big|_{y=0} - \frac{\partial}{\partial y} \Phi_{[n]}^{(1)} \Big|_{y=-\epsilon}}{\epsilon} \quad (6.20c)$$

$$R \{ e^{ikx} \}^2 = R \left\{ \frac{1}{2} + \frac{1}{2} e^{2ikx} \right\} \quad (6.21)$$

$$QFF = -2i\omega \frac{1}{2} \left(\frac{\partial \Phi_{[n]}^{(1)2}}{\partial y} + \frac{\partial \Phi_{[n]}^{(1)2}}{\partial x} \right) - \frac{1}{2} \eta_{[n]}^{(1)} \left(-\omega^2 \frac{\partial \Phi_{[n]}^{(1)}}{\partial y} + g \frac{\partial^2 \Phi_{[n]}^{(1)}}{\partial y^2} \right) \quad (6.22)$$

The results are compared to the analytical results of the quadratic forcing function from Chapter C, seen in Fig. 6.3. The differences are very small, and for increasing panel density these differences become smaller.

For clarity, the panels closest to the radiation condition have not been plotted. These values are not correct, which is a problem not related to the QFF calculation.

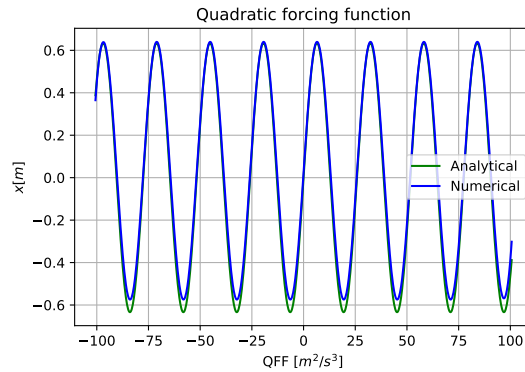


Figure 6.3: QFF on the free surface

Body boundary condition

The method is not developed far enough to place a body inside the domain and compare the results to existing literature, as the evanescent waves can not be found correctly yet. However, when the model is run with the body included and incorrect evanescent waves, the no-penetration boundary at the body is satisfied correctly.

Propagating wave results for model 1

The results for a propagating wave shows that the theoretical and numerical results still differ. In this example, a running wave is simulated in a domain of four wavelengths, with the properties as described in the introduction of this chapter. The results shown are the values of the first and second order potential at all boundaries.

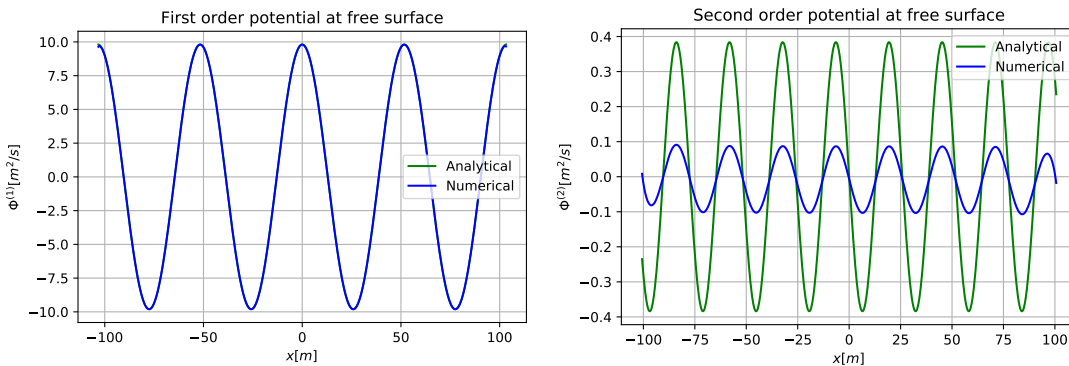


Figure 6.4: First and second order potential

The results show that the boundaries are not solved correctly. The first order potential is solved very accurately. The second order potential has some differences from the theoretical results.

Firstly, the amplitude at the free surface is not correct, as seen in Fig. 6.4. The frequency and wave length are correct, but the amplitude is too small. This could be related to the difference with the theoretical derivation to existing literature. The difference between the theoretical and numerical value is not a fixed ratio, but this is different for each water depth and wave frequency. Changes in the wave amplitude do not change the ratio of difference between the results. As a comparison, the right image shows the first order

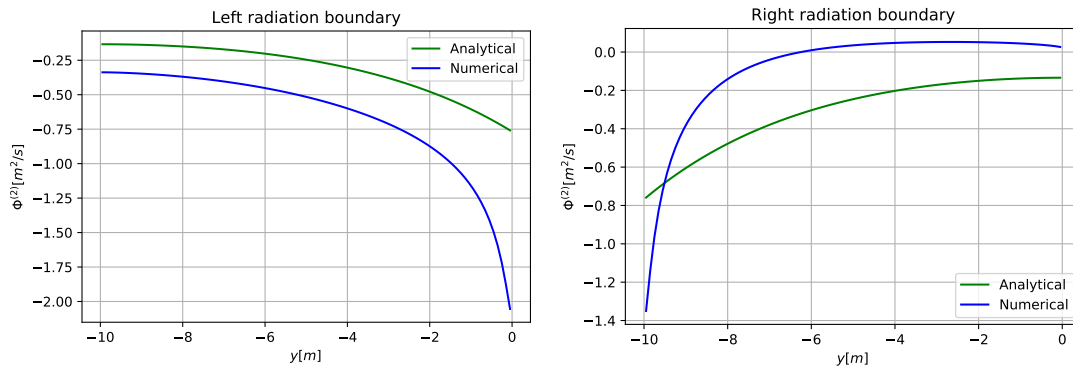


Figure 6.5: Second order potential on radiation boundaries

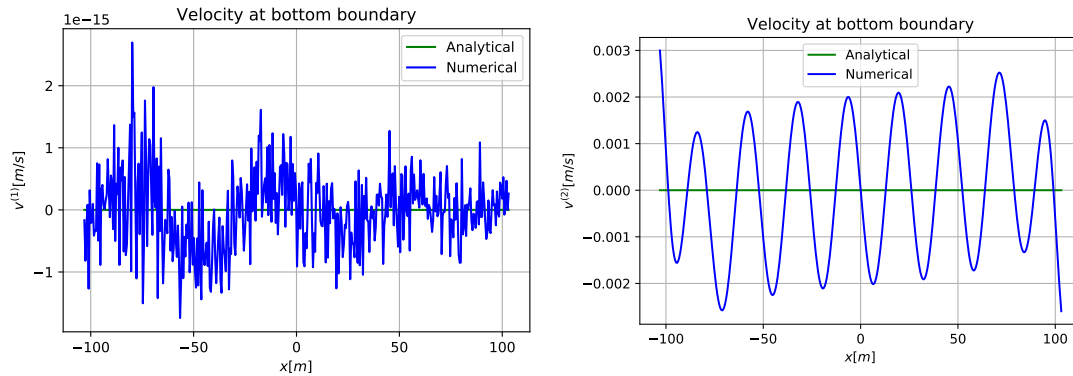


Figure 6.6: Second order potential on bottom boundary

solution, which is correct.

Secondly, the radiation boundaries are no longer accurate. It appears they suffer from the incorrect potential at the free surface, since the results are correct with a prescribed potential at the free surface boundary. In Fig. 6.5 it can be seen that for both the left and right boundary the values are no longer correct.

As seen in Fig. 6.6, the velocity at the bottom boundary is effectively 0 for the first order wave. The noise is probably caused by discretization and round-off errors, since they have a magnitude of 10^{-15} . The second order wave velocities do approach a solution where it is 0, but still shows some oscillations and the amplitude is quite large compared to the first order wave. The amplitude of these oscillations differ for different depths and frequencies.

Propagating wave results for model 2

The second model successfully runs a second order wave through the fluid domain. The results are shown below.

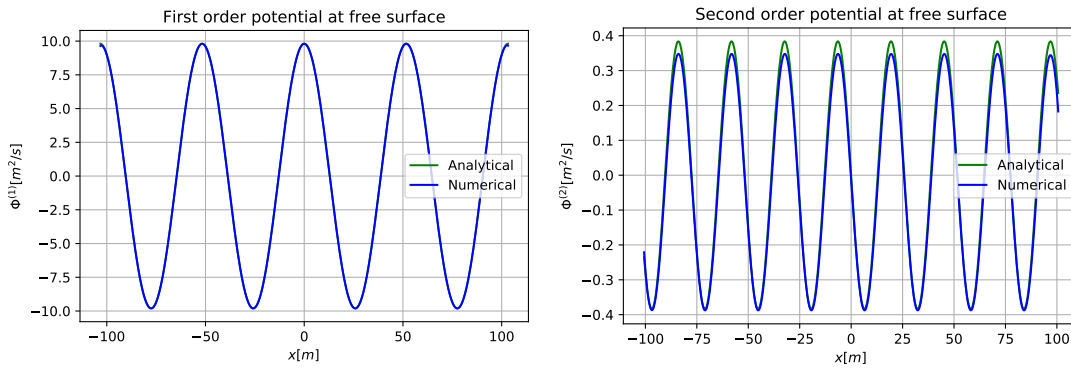


Figure 6.7: First and second order potential

It can be seen that both potential values are correct. There are small differences with regard to the second order amplitude. The peaks do not fully correspond with the analytical amplitude. This is however a small difference which reduces with increased panel density (this results is 100 panels per wave). From this result it can be concluded the $Q_{[n, m]}$ matrix has some difficulties finding the correct normal velocities on the free surface.

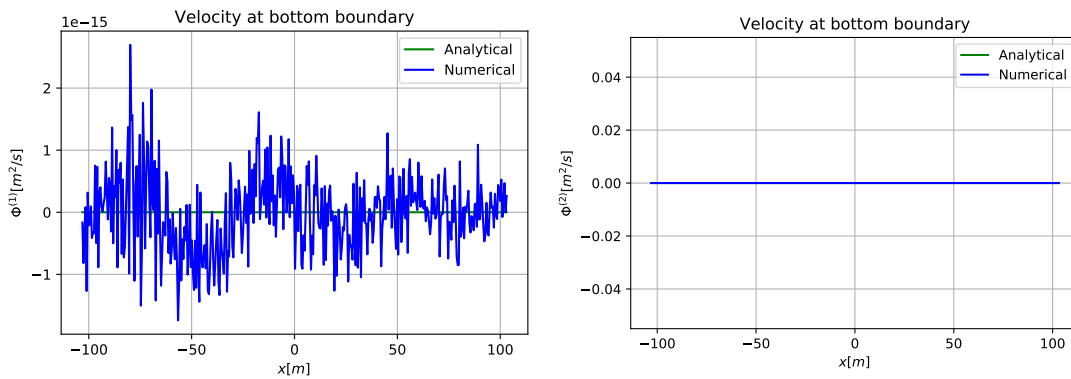


Figure 6.8: Second order potential on bottom boundary

The second order wave height is also determined from the derivation done by Stokes [24], as seen in Eq. (4.18). The comparison of the numerical and analytical results is shown below. A small difference for the linear result is visible, whereas the second order wave is well predicted. The result is shown in Fig. 6.9

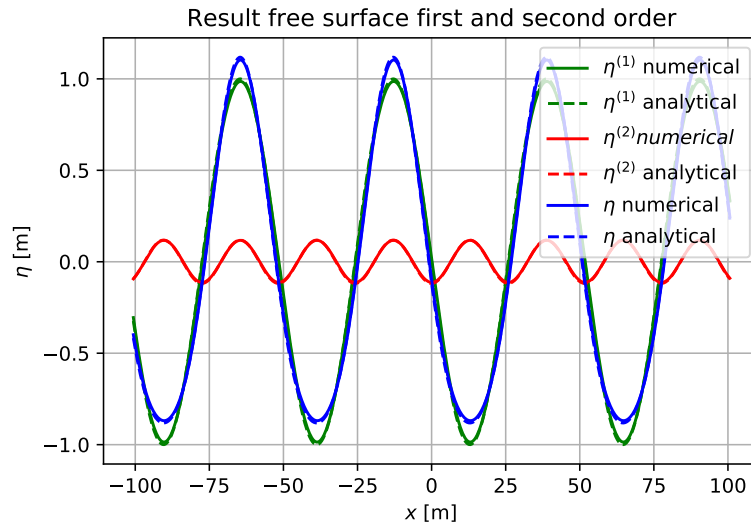


Figure 6.9: First and second order wave height

6.3 Conclusions

It has been shown that the second order model can successfully model the propagation of a second order wave through the domain. However, due to the way the $G_{[n,m]}$ matrix calculates the velocities at the free surface, it cannot be used for a problem containing evanescent waves. This means there will be errors in determining the normal velocities when a body is introduced in the domain.

The Sommerfeld condition can be used to generate a second order wave. However, since the linear wave is already present there is no absolute need to generate the second order wave, as the second order wave will already appear as a result of the QFF on the free surface. The successful results for the second order problem were generated without a Sommerfeld condition.

The complex numbers in the model used to describe the oscillations cannot simply be squared to find the QFF. This is because it represents a cosine only the real part should be squared. This has been successfully solved. Another challenge in finding the QFF was to find the double derivative in y . This has been solved with a numerical integration along the free surface which is also suitable for evanescent waves. The QFF calculation can therefore also be used with a body in the domain.

Chapter 7

Conclusions and recommendations

7.1 Conclusions

The conclusions to the research question and sub goals presented in Section 3.1 will be presented. The main goal of the thesis was to find the contribution of second order effects on the power prediction for wave energy converters.

How can the fluid domain be described?

In Section 2.1 different possibilities of finding wave loads in floating objects are found. It was concluded that a boundary element method with panels along all boundaries is the most applicable method. It allows the use of potential flow and to approximate an analytical solution by discretization. It does not provide a solution in the presence of any viscous forces, but these are small and outside the scope of this research. From the results presented in Section 5.7 it is shown the linear boundary conditions are successfully solved by the chosen method.

An error appears at the radiation and free surface boundaries, in the close proximity of their intersection point. This is seen in Section 5.7. The velocities tangential to the panels show different behaviour than expected from the linear wave theory. The cause of this error has not been found, but it does not influence the results of the energy prediction as all verification and validation on the body was successful.

The evanescent waves appear not to be affecting the radiation boundary if the radiation boundary is placed 0.5 wavelengths away from the body. This is for a linear wave, for a non-linear wave the behaviour should be re-evaluated.

How can a wave be added to the fluid domain?

A generating absorbing boundary condition is used. The absorbing boundary condition based on the Sommerfeld condition used by Yeung [31] was able to absorb waves, thus having waves leaving the domain. The GABC used by Wellens [30] for a CFD model was used on the radiation boundary where the wave enters the domain, with good success. The GABC accurately generates a wave entering the domain, as shown in Section 5.3.

How can the produced power of the moving body be determined?

The values of the potential, wave pattern, forces and hydro-dynamical properties can be found with success, as proven in Section 5.6. The power can be predicted with the theoretically derived optimal damping. It is also shown that energy conservation for the diffraction problem is achieved. The energy conservation for a coupled diffraction and radiation problem shows some energy losses. The reason for this energy loss has not been found. A small portion is due to discretization errors.

How can second order effects be implemented in the model?

The linear model is suitable to be extended with second order effects. The results and challenges are discussed in this chapter. The second order model is functional for a monochromatic wave running through the domain.

A challenge has been found in the pressure term found in Section 4.2. These pressure terms will interfere with the Sommerfeld condition when the incoming and reflected wave interact with each other. Possibly the Sommerfeld condition is not needed at all, but investigation on this behaviour with a body in the domain has not been performed.

The normal derivatives of the velocity on the free surface and quadratic forcing function are found with success in the BEM. With the boundary conditions given in the second model as shown in Section 6.1, the second order potential is solved successfully. The first model has trouble finding the correct amplitudes for the second order potential. This will create challenges when adding a body to the domain because of the evanescent waves.

7.2 Recommendations

Following this thesis, some recommendations are made for further research.

- Solve the problem with bi-chromatic waves. This also allows the calculation of second order drift forces on the body.
- Find a solution for the second order problem with a body. The current problem is that the evanescent waves cannot be correctly estimated at the free surface. A solution using a different method to find the normal velocities is required.
- Find a solution for the radiation boundary condition, as the pressure terms from incoming and reflected waves will induce pressure terms in the entire domain. A standard Sommerfeld condition does not take this pressure term into account, so an adapted solution needs to be found to model a GABC. A possible solution is that no radiation boundary is necessary for the second order problem, this remains to be investigated.
- Find a method to solve the diffraction and radiation problem simultaneously, as the incoming, reflected, transient and radiated waves interact with each other. This would require a coupling between both problems. The first order problem can be found completely by superimposing the radiation and diffraction solutions, which can then be used to find the second order terms using perturbation theory.
- Evaluate the second order behaviour of dampers used in a PTO. This will allow for a more precise power prediction and answer the main research question. Additional research on the non-linear behaviour of PTO dampers has to be done and implemented in the equations of motion from the BEM.

Bibliography

- [1] Panel Methods Source and Vortex, 2019.
- [2] Wave devices: EMEC European Marine Energy Centre, 2019.
- [3] A Ballast. *Water Waves, Fixed Cylinders and floating Spheres*. 2004.
- [4] V. Bertram. *Practical Ship Hydrodynamics*. 2012.
- [5] Z.S. Cheng, J.M. Yang, Z.Q. Hu, and L.F. Xiao. Frequency/time domain modeling of a direct drive point absorber wave energy converter. *Science China: Physics, Mechanics and Astronomy*, 57(2):311–320, 2014.
- [6] J. F. Dalzell. A note on finite depth second-order wave-wave interactions. *Applied Ocean Research*, 21(3):105–111, 1999.
- [7] W.R. Dean. On the reflexion of surface waves by a submerged plane barrier. *Mathematical Proceedings of the Cambridge Philosophical Society*, 41(3):231–238, 1948.
- [8] A. Falcão. Modelling and control of oscillating-body wave energy converters with hydraulic power take-off and gas accumulator. *Ocean Engineering*, 34(14-15):2021–2032, 2007.
- [9] W Frank. *Oscillations of Cylinders in or Below the Free Surface of Deep Fluids*. 1967.
- [10] L.H. Holthuisen. *Waves in Oceanic and Coastal Waters*. 2007.
- [11] M. Isaacson and J. Baldwin. Wave Propagation Past a Pile-Restrained Floating Breakwater. 8(4):1–5, 1998.
- [12] F. John. On The Motion of Floating Bodies. 12(5):1–5, 1949.
- [13] F. Kalofotias. Study for the Hull Shape of a Wave Energy Converter-Point Absorber Design Optimization & Modeling Improvement(M). (June):37, 2016.
- [14] M. Kim and D.K. Yue. The complete second-order diffraction solution for an axisymmetric body. Part 2. Bichromatic incident waves and body motions. *Journal of Fluid Mechanics*, 211:557–593, 1990.
- [15] Y. Kim, S.H. Kim, and T. Lucas. Advanced Panel Method for Ship Wave Inviscid Flow Theory (SWIFT). 1989.
- [16] R Kincaid. Effects of natural period upon the characteristics of a moored floating breakwater. 1960.
- [17] P.K. Kundu. *Fluid Mechanics - Sixth Edition*. 2016.
- [18] M. S. Longuet-Higgins. Resonant interactions between two trains of gravity waves. *Journal of Fluid Mechanics*, 12(3):321–332, 1962.
- [19] C.C. Mei. *The Applied Dynamics of Ocean Surface Waves*. 1983.
- [20] C.C. Mei and J.L. Black. Scattering of surface waves by rectangular obstacles in waters of finite depth. *Journal of Fluid Mechanics*, 38(3):499–511, 1969.
- [21] B. Molin. Second-order diffraction loads upon three-dimensional bodies. *Applied Ocean Research*, 1(4):197–202, 1979.

- [22] J.N. Newman. Marine Hydrodynamics - Waves and Wave Effects (Ch. 6). *Marine hydrodynamics*, pages 237–327, 1977.
- [23] T. Francis Ogilvie. First- and second-order forces on a cylinder submerged under a free surface. *Journal of Fluid Mechanics*, 16(3):451–472, 1963.
- [24] G.G. Stokes. On the Theory of Oscillatory Waves. *Mathematical and Physical Papers*, 1:225–28, 1847.
- [25] B. Teillant, J. C. Gilloteaux, and J. V. Ringwood. *Optimal damping profile for a heaving buoy wave energy converter*, volume 43. IFAC, 2010.
- [26] F. Ursell. The effect of a fixed vertical barrier on surface waves in deep water. 1947.
- [27] F Ursell. on the Heaving Motion of a Circular Cylinder on the Surface of a Fluid. (April 1948), 1949.
- [28] F. Ursell and W. R. Dean. Surface waves on deep water in the presence of a submerged circular cylinder. *Mathematical Proceedings of the Cambridge Philosophical Society*, 46(01):153, 1950.
- [29] P. R. Wellens. Wave Energy – Study to determine the optimal performance of a floating wave energy converter. 2004.
- [30] P. R. Wellens. *Wave Simulation in Truncated Domains for Offshore Applications*. PhD thesis, 2012.
- [31] R.W. Yeung. A singularity-distribution method for free surface flow problems with an oscillating body. (August), 1973.
- [32] X. Zhao, D. Ning, C. Zhang, and H. Kang. Hydrodynamic investigation of an oscillating buoy wave energy converter integrated into a pile-restrained floating breakwater. *Energies*, 10(5), 2017.

Appendices

Appendix A

Green Function

Green functions are used to describe the influence of a (pulsating) source positioned at \mathbf{x}_0 on the fluid domain. The simplest form of a Green function would be of a source with constant strength q , as seen in Eq. (A.1). This Green function is used to describe the influence of the source on the entire fluid domain, and can satisfy the boundary conditions with a source strength which is to be calculated.

$$G(\mathbf{x}|\mathbf{x}_0) = \frac{q}{2\pi} \ln |\mathbf{x} - \mathbf{x}_0| = \frac{q}{2\pi} \ln r \quad (\text{A.1})$$

When the Green function must also satisfy the free-surface boundary condition, it becomes more complicated. A good derivation is found by Mei [19], and the most critical steps will be discussed in this chapter.

The Green function is derived from Greens theorem, which is seen in Eq. (A.2). For a 2D potential flow problem, where $\nabla^2 G = \delta(\mathbf{x} - \mathbf{x}_0)$, this can be simplified to Eq. (A.5) using the Dirac property as seen in Eq. (A.4), with the singularity at \mathbf{x}_0 included in S . Also, symmetry is used to interchange \mathbf{x} with \mathbf{x}_0 .

$$\iint_{\Omega} (\Phi \nabla^2 G - G \nabla^2 \Phi) d\Omega = \iint_{d\Omega} \left(\Phi \frac{\partial G}{\partial n} - G \frac{\partial \Phi}{\partial n} \right) dS \quad (\text{A.2})$$

$$\iint_{\Omega} (\Phi \nabla^2 G) d\Omega = \int_S \left(\Phi \frac{\partial G}{\partial n} - G \frac{\partial \Phi}{\partial n} \right) dS \quad (\text{A.3})$$

$$\int_S f(x) \delta(x - a) dS = f(a) \quad (\text{A.4})$$

$$\Phi(\mathbf{x}) = \int_S \left(\Phi(\mathbf{x}_0) \frac{\partial G}{\partial n} - G \frac{\partial \Phi(\mathbf{x}_0)}{\partial n} \right) dS \quad (\text{A.5})$$

The Green function must satisfy the boundary conditions as seen in Eq. (A.6), where (x_0, y_0) is the source location. Eq. (A.6a) shows the Laplace equation. The only place where a source is not actually an ideal flow is at the singularity of the source location. Since this singularity is not within the flow field that is being solved, but within or on the body, this does not impose a problem for the solution. This singularity will be seen as a Dirac function for the Laplace equation. Eq. (A.6b) is a representation of the linear free surface boundary condition and Eq. (A.6c) is the radiation condition at infinity.

$$\frac{\partial^2 G}{\partial x^2} + \frac{\partial^2 G}{\partial y^2} = \delta(x - x_0) \delta(y - y_0) \quad (\text{A.6a})$$

$$\frac{\partial G}{\partial y} - \omega G = 0 \quad (y = 0) \quad (\text{A.6b})$$

$$\frac{\partial G}{\partial x} \pm ikG = 0 \quad (k|x - x_0| \rightarrow \infty) \quad (\text{A.6c})$$

If these conditions are made for the Fourier transform of G with respect to x , the following equations are obtained, where K is the Fourier transform variable:

$$\frac{\partial^2 \tilde{G}}{\partial y^2} - K^2 \tilde{G} = \delta(y - y_0) e^{-iKx_0} \quad -\infty < y < 0, y \neq y_0 \quad (\text{A.7a})$$

$$\tilde{G}|_{z+z_0^+} - \tilde{G}|_{z+z_0^-} = 0 \quad (\text{A.7b})$$

$$\frac{\partial \tilde{G}}{\partial y}|_{z+z_0^+} - \frac{\partial \tilde{G}}{\partial y}|_{z+z_0^-} = e^{-iKx_0} \quad (\text{A.7c})$$

$$\frac{\partial \tilde{G}}{\partial y} - \omega \tilde{G} = 0 \quad (y = 0) \quad (\text{A.7d})$$

The solution to this problem can be presented in the form of Eq. (A.8), where the function $\tilde{w}(\mathbf{x}, \mathbf{x}_0)$ represents the solution to the boundary conditions above.

$$\tilde{G} = e^{-iKx_0} \tilde{w}(\mathbf{x}, \mathbf{x}_0) \quad (\text{A.8})$$

When taking the Fourier inverse of this function, a problem arises with the integral. The Fourier inverse formula is given in Eq. (A.9). Since the function of \tilde{w} is symmetric, the integral can be taken as twice the integral from 0 to ∞ . The problem is the integration of the poles (singularities) at $K = \pm k$ and $K = \pm ik$.

$$f(x) = \frac{1}{2\pi} \int_{-\infty}^{\infty} \tilde{f}(K) e^{iKx} dK \quad (\text{A.9})$$

$$G(\mathbf{x}, \mathbf{x}_0) = \frac{1}{\pi} \int_0^{\infty} e^{iK(x-x_0)} \tilde{w}(\mathbf{x}, \mathbf{x}_0) dK \quad (\text{A.10})$$

These singularities are solved using the Cauchy theorem. This shows that for a function with a singularity at z_j , the complex function of $f(z)$ can be solved with the residue theorem, if z_j is with the integrated domain. In Eq. (A.11), N is the number of poles, n is the order of singularity and z_j is the complex pole location.

$$\oint_c f(z) dz = 2\pi i \sum_{j=1}^N \text{Res}(f(z)|_{z=z_j}) \quad (\text{A.11})$$

$$\text{Res}(f(z)|_{z=z_j}) = \frac{1}{(n-1)!} \lim_{z \rightarrow z_j} \frac{\partial^{n-1}}{\partial z^{n-1}} [(z-z_j)^n f(z)] \quad (\text{A.12})$$

It is logical that near the source point, the source point will dominate the function. Knowing the potential function for a source, given in Eq. (A.14), and with the use of the Laplace transform identities shown in Eq. (A.15) the final expression for G can be derived. The derivation depends strongly on the function \tilde{w} .

$$|\mathbf{x} - \mathbf{x}_0| = r \quad (\text{A.13})$$

$$\Phi = \frac{Q}{2\pi} \ln r \quad (\text{A.14})$$

$$\int_0^{\infty} \frac{dK}{K} e^{-Kb} (1 - \cos Ka) = \ln \left[\frac{\sqrt{a^2 + b^2}}{b} \right] \quad (\text{A.15a})$$

$$\int_0^{\infty} \frac{dK}{K} (e^{-Kb} - e^{-Kh}) = \ln \frac{h}{b} \quad (\text{A.15b})$$

The resulting Green function for a linear problem in deep water is seen in Eq. (A.16). The first term is the source at the body and the second term satisfies the linear free surface boundary conditions as seen in Eq. (A.6). For more details refer to Mei [19] or John [12]. For a higher order free surface boundary condition the derivation could become complicated quickly.

$$G(\mathbf{x}, \mathbf{x}_0) = \frac{2}{\pi} \ln r + \int_0^{\infty} \frac{dK}{K} \left[\frac{\omega + K}{\omega - K} e^{K(y+y_0)} \cos K(x-x_0) - e^{-K} \right] \quad (\text{A.16})$$

Added mass & damping coefficients

Mei [19] derived the added mass and damping matrix from the radiated waves. This begins by separating the radiation potential by different modes. For the notation in this report it is simplified to two dimensions. The definition is as follows, with α the different modes (1 for surge, 3 for heave and 5 for pitch):

$$\Phi_R = \sum_{\alpha} v_{\alpha} \phi_{\alpha}, \quad (\text{A.17})$$

in which v_{α} represents the amplitude of the body velocity in mode α . The hydrodynamic force on the body is also generalised. The complex notation is seen in Eq. (A.18).

$$\int_{S_B} p n_{\alpha} dS = \text{Re}\{F_{\alpha} e^{-i\omega t}\} \quad (\text{A.18})$$

$$F_{\alpha} = i\rho\omega \int_{S_B} \Phi n_{\alpha} dS \quad (\text{A.19})$$

$$F_{\alpha} = i\rho\omega \int_{S_B} \Phi_D n_{\alpha} dS + \sum_{\beta} i\rho\omega v_{\beta} \int_{S_B} \phi_{\beta} n_{\alpha} dS \quad (\text{A.20})$$

Where β represents a mode ($\beta = 1, 3, 5$)

$$F_{\alpha} = F_{\alpha}^D + \sum_{\beta} v_{\beta} f_{\beta\alpha} \quad (\text{A.21})$$

In this final equation, F_{α}^D represents the exciting force due to diffraction. $f_{\beta\alpha}$ is the restoring force matrix, where $(\beta\alpha)$ is the component that represents a hydrodynamic reaction in mode α due to normal mode β . This component can be evaluated further to find the added mass and damping components (without summing over β):

$$\text{Re}\{v_{\beta} f_{\beta\alpha} e^{-i\omega t}\} = \text{Re}\{(Re f_{\beta\alpha} + i Im f_{\beta\alpha}) v_{\beta} e^{-i\omega t}\} \quad (\text{A.22a})$$

$$= \text{Re}\left\{\left(i\rho\omega \int_{S_B} Re \phi_{\beta} n_{\alpha} dS - \rho\omega \int_{S_B} Im \phi_{\beta} n_{\alpha} dS\right) v_{\beta} e^{-i\omega t}\right\} \quad (\text{A.22b})$$

$$= -\left(\rho \int_{S_B} Re \phi_{\beta} n_{\alpha} dS\right) \text{Re} \frac{\partial}{\partial t} (v_{\beta} e^{-i\omega t}) - \left(\rho\omega \int_{S_B} Im \phi_{\beta} n_{\alpha} dS\right) \text{Re}(v_{\beta} e^{-i\omega t}) \quad (\text{A.22c})$$

$$= -\left(\rho \int_{S_B} Re \phi_{\beta} n_{\alpha} dS\right) \ddot{X}_{\beta} - \left(\rho\omega \int_{S_B} Im \phi_{\beta} n_{\alpha} dS\right) \dot{X}_{\beta} \quad (\text{A.22d})$$

$$= [\mu] \ddot{X}_{\beta} + [\lambda] \dot{X}_{\beta} \quad (\text{A.22e})$$

$$F_{\alpha}^R = -\sum_{\beta} \mu_{\beta\alpha} \ddot{X}_{\beta} - \sum_{\beta} \lambda_{\beta\alpha} \dot{X}_{\beta} \quad (\text{A.23})$$

Eq. (A.23) shows the expressions for the added mass matrix $[\mu]$ and the radiation damping matrix $[\lambda]$. These can then be substituted into a simple equation of motion as seen in Eq. (A.24), with ξ as amplitude of a regular motion.

$$[-\omega^2([M] + [\mu]) + [C] - i\omega[\lambda]] \{\xi\} = \{F^D\} + \{F_{ext}\} \quad (\text{A.24})$$

These equations are all linear. For a second order system, they should be expanded using Taylor expansions or other methods.

Appendix B

Derivation Linear Potential

For a full derivation of the linear wave potential for finite and infinite depth refer to Mei [19] or Holthuizen [10]. Some more details on linear waves are found below.

Free surface

The free surface is found from the dynamic and kinematic boundary conditions, resulting in the following equation for the wave height:

$$\eta = -\frac{1}{g} \frac{\partial \Phi}{\partial t} \quad (\text{B.1})$$

$$\eta = A \sin(\omega t - kx) \quad (\text{B.2})$$

Left going wave

A wave propagating in the negative x-direction is called a left going wave. This is defined slightly differently as the right going wave:

$$\Phi = \frac{A \omega}{k} \frac{\cosh(k(h+y))}{\cosh(kh)} \cos(\omega t + kx) \quad (\text{B.3})$$

Second order boundary conditions

The second order potential is derived from the Bernoulli equation at the free surface. At the free surface, the pressure is equal to the atmospheric pressure. The Bernoulli equation is shown in Eq. (B.4) below. The resulting expression for the wave height is found by evaluating this from the strong form of the Bernoulli equation. The characteristic of the strong form is that potential flow is used and the equation is a constant in the entire domain. Therefore, the pressure can be eliminated and the constant can be chosen as 0. Substituting the wave height for y gives the pressure at the free surface.

$$\frac{p}{\rho} = \frac{\partial \Phi}{\partial t} + \frac{1}{2} \nabla \Phi \cdot \nabla \Phi + gy = 0 \quad (\text{B.4})$$

$$\eta = -\frac{1}{g} \left(\frac{\partial \Phi}{\partial t} + \frac{1}{2} \nabla \Phi \cdot \nabla \Phi \right) \quad (\text{B.5})$$

At the free surface, the material derivative of the pressure is 0. the material derivative is the change of the pressure when following a particle. This results in the free surface boundary condition

$$\frac{Dp}{Dt} = 0 \quad y = \eta \quad (\text{B.6a})$$

$$\left(\frac{\partial}{\partial t} + \nabla \Phi \cdot \nabla \right) \left(\frac{\partial \Phi}{\partial t} + \frac{1}{2} \nabla \Phi \cdot \nabla \Phi + gy \right) = 0 \quad (\text{B.6b})$$

This results in 5 terms from the product sum rule. Numbering the individual terms from Eq. (B.6b) from 1 to 5, the results are shown below. The final boundary condition for the free surface, a sum of these individual terms, is shown in Eq. (B.8). The third order term is cancelled out.

$$(1, 3) : \frac{\partial^2 \Phi}{\partial t^2} \quad (\text{B.7a})$$

$$(1, 4) : \frac{1}{2} \frac{\partial}{\partial t} (\nabla \Phi \cdot \nabla \Phi) = \nabla \Phi \cdot \nabla \frac{\partial \Phi}{\partial t} \quad (\text{B.7b})$$

$$(1, 5) : 0 \quad (\text{B.7c})$$

$$(2, 3) : \nabla \Phi \cdot \nabla \frac{\partial \Phi}{\partial t} \quad (\text{B.7d})$$

$$(2, 4) : \frac{1}{2} \nabla \Phi \cdot \nabla (\nabla \Phi \cdot \nabla \Phi) \quad (\text{B.7e})$$

$$(2, 5) : g \frac{\partial \Phi}{\partial y} \quad (\text{B.7f})$$

$$\frac{\partial^2 \Phi}{\partial t^2} + g \frac{\partial \Phi}{\partial y} + 2 \nabla \Phi \cdot \nabla \frac{\partial \Phi}{\partial t} + \frac{1}{2} \nabla \Phi \cdot \nabla (\nabla \Phi \cdot \nabla \Phi) = 0 \quad (\text{B.8})$$

As a next step, a Taylor expansion is made around $y=0$ to approximate the potential on the free surface. Again, third order terms are cancelled out.

$$\Phi(x, \eta, t) = \Phi(x, 0, t) + \eta \frac{\partial \Phi}{\partial y} |_{y=0} \quad (\text{B.9a})$$

$$0 = \frac{\partial^2 \Phi}{\partial t^2} + g \frac{\partial \Phi}{\partial y} + 2 \nabla \Phi \cdot \nabla \frac{\partial \Phi}{\partial t} + \eta \frac{\partial}{\partial y} \left(\frac{\partial^2 \Phi}{\partial t^2} + g \frac{\partial \Phi}{\partial y} + \cancel{2 \nabla \Phi \cdot \nabla \frac{\partial \Phi}{\partial t}} \right) \quad (\text{B.9b})$$

$$0 = \frac{\partial^2 \Phi}{\partial t^2} + g \frac{\partial \Phi}{\partial y} + 2 \nabla \Phi \cdot \nabla \frac{\partial \Phi}{\partial t} - \frac{1}{g} \left(\frac{\partial \Phi}{\partial t} + \frac{1}{2} \nabla \Phi \cdot \nabla \Phi \right) \frac{\partial}{\partial y} \left(\frac{\partial^2 \Phi}{\partial t^2} + g \frac{\partial \Phi}{\partial y} \right) \quad (\text{B.9c})$$

$$0 = \frac{\partial^2 \Phi}{\partial t^2} + g \frac{\partial \Phi}{\partial y} + 2 \nabla \Phi \cdot \nabla \frac{\partial \Phi}{\partial t} - \frac{1}{g} \frac{\partial \Phi}{\partial t} \frac{\partial}{\partial y} \left(\frac{\partial^2 \Phi}{\partial t^2} + g \frac{\partial \Phi}{\partial y} \right) \quad (\text{B.9d})$$

Next, the potential is split in a first and second order term. For both orders a separate equation appears. All terms leading to terms higher than second order are left out.

$$\Phi = \Phi^{(1)} + \Phi^{(2)} \quad (\text{B.10a})$$

$$\frac{\partial^2 \Phi^{(1)}}{\partial t^2} + g \frac{\partial \Phi^{(1)}}{\partial y} + \frac{\partial^2 \Phi^{(2)}}{\partial t^2} + g \frac{\partial \Phi^{(2)}}{\partial y} + 2 \nabla \Phi^{(1)} \cdot \nabla \frac{\partial \Phi^{(1)}}{\partial t} - \frac{1}{g} \frac{\partial \Phi^{(1)}}{\partial t} \frac{\partial}{\partial y} \left(\frac{\partial^2 \Phi^{(1)}}{\partial t^2} + g \frac{\partial \Phi^{(1)}}{\partial y} \right) = 0 \quad (\text{B.10b})$$

$$\frac{\partial^2 \Phi^{(1)}}{\partial t^2} + g \frac{\partial \Phi^{(1)}}{\partial y} = 0 \quad (\text{B.10c})$$

$$\frac{\partial^2 \Phi^{(2)}}{\partial t^2} + g \frac{\partial \Phi^{(2)}}{\partial y} = -2 \nabla \Phi^{(1)} \cdot \nabla \frac{\partial \Phi^{(1)}}{\partial t} + \frac{1}{g} \frac{\partial \Phi^{(1)}}{\partial t} \frac{\partial}{\partial y} \left(\frac{\partial^2 \Phi^{(1)}}{\partial t^2} + g \frac{\partial \Phi^{(1)}}{\partial y} \right) \quad (\text{B.10d})$$

For deep water waves in Eq. (B.10d), the right hand side reduces to 0 analytically, for the potential found in Eq. (4.2b). This means the first order potential is a solution to the second order problem and the second order term for monochromatic deep water waves disappears.

Appendix C

Finite depth second order wave derivation

In finite depth, the second order potential is not zero. This second order term can be derived from the boundary conditions. At the free surface, the following boundary condition, known first order potential and dispersion relation are the beginning of the derivation. The dispersion relation is a solution to the linear free surface boundary condition, as shown by Newman [22]. This derivation is based on Stokes [24]. The derivation is done in the frame of reference moving along with the wave.

$$x' = x - c t \quad (\text{C.1a})$$

$$x = x' \quad (\text{C.1b})$$

$$\Phi^{(1)} = A \cosh(k(h + y)) \sin(k x) \quad (\text{C.1c})$$

$$c^2 \frac{\partial^2 \Phi^{(2)}}{\partial x^2} + g \frac{\partial \Phi^{(2)}}{\partial y} = -2 \nabla \Phi^{(1)} \cdot \nabla (-c) \frac{\partial \Phi^{(1)}}{\partial x} + \frac{-c}{g} \frac{\partial \Phi^{(1)}}{\partial x} \frac{\partial}{\partial y} \left(c^2 \frac{\partial^2 \Phi^{(1)}}{\partial x^2} + g \frac{\partial \Phi^{(1)}}{\partial y} \right) \quad (\text{C.1d})$$

$$c^2 = \frac{g}{k} \tanh(k h) \quad (\text{C.1e})$$

The right hand side of Eq. (C.1d) is evaluated first.

$$-2 \nabla \Phi^{(1)} \cdot \nabla (-c) \frac{\partial \Phi^{(1)}}{\partial x} = c \frac{\partial}{\partial x} (\nabla \Phi^{(1)} \cdot \nabla \Phi^{(1)}) \quad (\text{C.2a})$$

$$= c \frac{\partial}{\partial x} \left(\frac{\partial \Phi^{(1)^2}}{\partial x} + \frac{\partial \Phi^{(1)^2}}{\partial y} \right) \quad (\text{C.2b})$$

$$\frac{\partial \Phi^{(1)^2}}{\partial x} = A^2 k^2 \cosh^2(k(h + y)) \cos^2(k x) \quad (\text{C.2c})$$

$$\frac{\partial \Phi^{(1)^2}}{\partial y} = A^2 k^2 \sinh^2(k(h + y)) \sin^2(k x) \quad (\text{C.2d})$$

$$\left(\frac{\partial \Phi^{(1)^2}}{\partial x} + \frac{\partial \Phi^{(1)^2}}{\partial y} \right) = A^2 k^2 (\cosh^2(k(h + y)) + \cos^2(k x) - 1) \quad (\text{C.2e})$$

$$c \frac{\partial}{\partial x} \left(\frac{\partial \Phi^{(1)^2}}{\partial x} + \frac{\partial \Phi^{(1)^2}}{\partial y} \right) = -c A^2 k^3 \sin(2 k x) \quad (\text{C.2f})$$

$$\frac{-c}{g} \frac{\partial \Phi^{(1)}}{\partial x} = \frac{-c A k}{g} \cosh(k(h+y)) \cos(kx) \mid y=0 \quad (\text{C.3a})$$

$$c^2 \frac{\partial^2 \Phi^{(1)}}{\partial x^2} = -c^2 A k^2 \cosh(k(h+y)) \sin(kx) \quad (\text{C.3b})$$

$$g \frac{\partial \Phi^{(1)}}{\partial y} = g A \sinh(k(h+y)) \sin(kx) \quad (\text{C.3c})$$

$$\frac{\partial}{\partial y} \left(c^2 \frac{\partial^2 \Phi^{(1)}}{\partial x^2} + g \frac{\partial \Phi^{(1)}}{\partial y} \right) = A \sin(kx) k^2 (-\sinh(k(h+y)) c^2 k + \cosh(k(h+y)) g) \quad (\text{C.3d})$$

$$\frac{-c}{g} \frac{\partial \Phi^{(1)}}{\partial x} \frac{\partial}{\partial y} \left(c^2 \frac{\partial^2 \Phi^{(1)}}{\partial x^2} + g \frac{\partial \Phi^{(1)}}{\partial y} \right) = \quad (\text{C.3e})$$

$$= -\frac{c^5 A^2 k^5 \cos(kx) \sin(kx) \cosh(kh)^2}{g^2 \sinh(kh)^2} \quad (\text{C.3f})$$

The boundary condition with substitution of the dispersion relation then becomes:

$$c^2 \frac{\partial^2 \Phi^{(2)}}{\partial x^2} + g \frac{\partial \Phi^{(2)}}{\partial y} = -c A^2 k^3 \sin(2kx) + -\frac{c^5 A^2 k^5 \cos(kx) \sin(kx) \cosh(kh)^2}{g^2 \sinh(kh)^2} \quad (\text{C.4a})$$

$$= -\frac{3c A^2 k^3 \sin(2kx)}{2} \quad (\text{C.4b})$$

The second order potential has the following characteristic, the challenge is to find B.

$$\Phi^{(2)} = B \cosh(2k(h+y)) \sin(2kx) \quad (\text{C.5})$$

Again, with substitution of the dispersion relation the equation for the second order becomes as shown.

$$-8Bk^2 \sinh(kh)^2 \sin(2kx) c^2 = -\frac{3c A^2 k^3 \sin(2kx)}{2} \quad (\text{C.6a})$$

$$B = \frac{3A^2 k}{16c \sinh(kh)^2} \quad (\text{C.6b})$$

From the first order potential, A is known to be:

$$A = \frac{ca}{\sinh(kh)} \quad (\text{C.7})$$

This results in the following second order potential:

$$\Phi^{(2)} = \frac{3ca^2 k \cosh(2k(h+y)) \sin(2kx)}{8 \sinh(kh)^4} \quad (\text{C.8})$$

Appendix D

Boundary element method

About the method

A panel method is a method to satisfy boundary conditions within a flow. The flow is disrupted by a body in the flow, made up from panels. Each panel is a location on which the boundary conditions must be satisfied. This helps breaking down a complicated boundary condition to a matrix problem.

Source Panels

Simply put, a panel method consists of a kind of source for each panel which satisfies the boundary condition at that panel. However, when a source creates a flow, it also influences the entire fluid domains and therefore all other panels. These influences are all captured in a matrix, the influence matrix, which will be come back to later.

$$z = x + iy \quad (D.1)$$

$$W(z) = u - iv \quad (D.2)$$

Eq. (D.1) describes the coordinate z in complex coordinates. Eq. (D.2) shows the complex velocity.

$$W(z) = \frac{q}{2\pi(z - z_1)} \quad (D.3)$$

Creating a linear panel method is done in smaller steps. First, an example is made for a steady uniform flow. A typical source description is given in Eq. (D.3), where q is the source strength, z any coordinate and z_1 the source coordinate. To reduce velocity peaks and strong variation in the velocity along the panel, the source strength is integrated along the panel surface to create a panel source as seen in Fig. D.1. A point source and a panel source are both shown on the left, with the local coordinate s shown on the right. The velocity field for a constant source strength along the panel is as follows:

$$W(z) = \frac{1}{2\pi} \int_{panel} \frac{q ds}{z - z_1(s)} \quad (D.4)$$

with $0 \leq s \leq 1$ describing the panel:

$$z_1(s) = z_a + s(z_b - z_a) \quad (D.5)$$

$$\frac{dz}{ds} = e^{i\beta} = \frac{z_b - z_a}{|z_b - z_a|} \quad (D.6)$$

The angle of the source panel with respect to the x,y coordinate system is calculated in Eq. (D.6). This is used to change the global velocities from the panel source to velocities normal and tangential to the panel. This is especially useful for a no normal velocity boundary condition, which will be applied to each panel.

$$v_s - iv_n = W(z) \frac{dz_1}{ds} = \frac{q}{2\pi} \ln \left(\frac{z - z_a}{z - z_b} \right) \quad (D.7)$$

This panel is not yet a solid boundary. This is achieved then the strength q is chosen so that the total v_n is zero (from the panel and external flow).

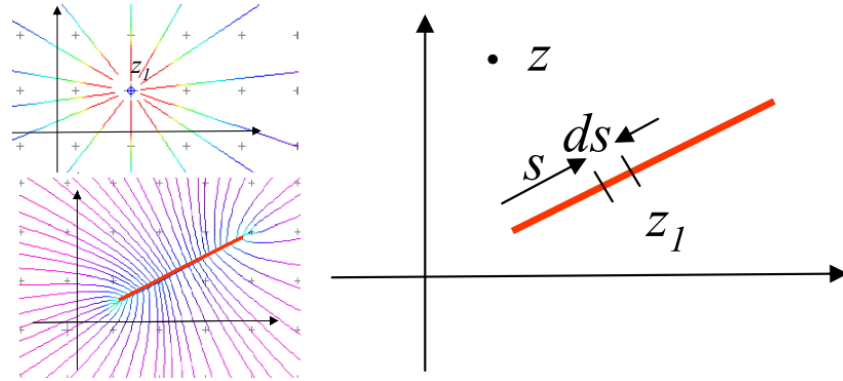


Figure D.1: Source Panel [1]

Collocation Points

Collocation points are added to each panel. These points are used for the calculation of the panel strength, so that no integration is needed for that step. The collocation point is placed just within the body close to the panel, as a point on the panel would result in a singularity from the panel source itself. It is defined as follows and seen in Fig. D.2:

$$z_c = \frac{1}{2}(z_a + z_b) - i\epsilon(z_b - z_a) \quad (D.8)$$

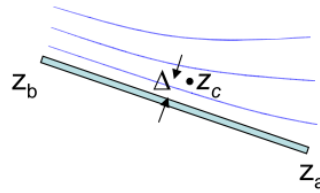


Figure D.2: Collocation Point [1]

ϵ is a sufficiently small number, for example 10^{-4} . The displacement Δ is then given by the second term in the equation for z_c . This collocation point is used to determine the flow from the entire body on the panel, and it is on this point that the boundary conditions are satisfied.

Influence Matrix

As previously mentioned, the influence matrix describes the influence of each panel on all other panels. The velocity at the control point of panel m due to all other panels n is shown in Eq. (D.9), in the coordinates aligned with the panel.

$$v_s - iv_n = \sum_{n=1}^N q^{(n)} \frac{1}{2\pi} \ln \left(\frac{z_c^{(m)} - z_a^{(n)}}{z_c^{(m)} - z_b^{(n)}} \right) \frac{ds}{dz_1} \Big|^{(n)} \frac{dz_1}{ds} \Big|^{(m)} \quad (D.9)$$

$$V^{(m,n)} = \sum_{n=1}^N \frac{1}{2\pi} \ln \left(\frac{z_c^{(m)} - z_a^{(n)}}{z_c^{(m)} - z_b^{(n)}} \right) \frac{ds}{dz_1} \Big|^{(n)} \frac{dz_1}{ds} \Big|^{(m)} \quad (D.10)$$

Imagine the influence of a panel on its own collocation point ($n=m$). In this case, half the flow from the source will go through that point, whereas the other half will go outside of the body. Therefore, the diagonals of the influence matrix should always be $0.5i$. This also makes the matrix diagonally dominant, which allows for reliable matrix division.

The external flow can be written to the local coordinates of the panel as well, as seen below:

$$v_s - iv_n = W_\infty \frac{dz_1}{ds} \Big|^{(m)} \quad (\text{D.11})$$

This allows to write the normal velocity and tangential velocity as the imaginary and real parts of the combination of the external velocity and the velocities created by the panels.

$$v_s = \text{Re} \left\{ \frac{dz_1}{ds} \Big|^{(m)} W_\infty \right\} + \sum_{n=1}^N q^{(n)} \text{Re}\{V^{(m,n)}\} \quad (\text{D.12a})$$

$$v_n = \text{Im} \left\{ \frac{dz_1}{ds} \Big|^{(m)} W_\infty \right\} + \sum_{n=1}^N q^{(n)} \text{Im}\{V^{(m,n)}\} \quad (\text{D.12b})$$

A different notation is used for the normal velocity influence matrix:

$$\text{Im}\{V^{(m,n)}\} = Q^{(m,n)} \quad (\text{D.13})$$

Source Strengths

Finally, the goal is to satisfy the boundary condition of no flow through each panel $v_n^{(n)} = 0$. This results in the matrix division as seen below:

$$q^{(n)} = -\text{Im} \left\{ \frac{dz_1}{ds} \Big|^{(m)} W_\infty \right\} / Q^{(m,n)} \quad (\text{D.14})$$

The challenge is to find the right influence matrix for more difficult boundary conditions and external flows, such as a free surface and a non-uniform incoming flow with oscillating behaviour. This will result in a different $W(z)$ for the panels (instead of only a source) and possibly additional panels at additional boundaries. The essence of solving the boundary on the panel will remain the same however. Knowing the source strengths q for each panel, the total flow can be found. For a cylinder with 35 panels, this results in Fig. D.3. The flow inside the cylinder has no physical meaning.

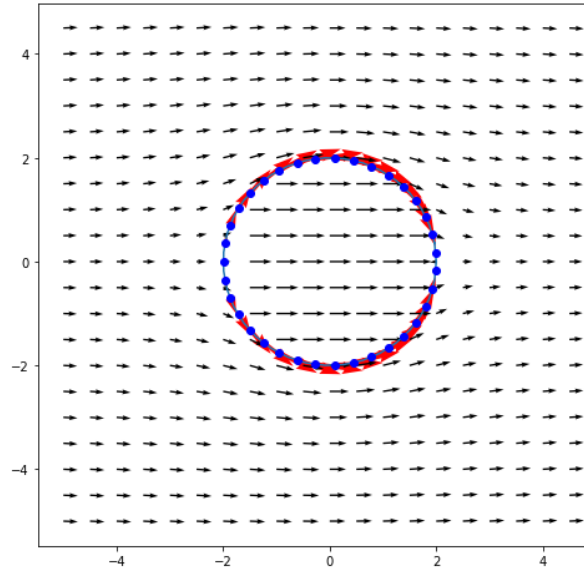


Figure D.3: Steady flow around a cylinder

Boundary Value Problem

For a boundary-value problem only with a moving body, without a prescribed velocity field as seen above, the resulting boundary condition is:

$$\sum_{S_b} q^{(n)} Q^{(n,m)} = \hat{n}^{(n)} \cdot \mathbf{u}_b^{(n)} \quad (\text{D.15})$$